

Anomalous wide angle X-ray scattering (AWAXS) and heterogeneous catalysts

D. Bazin^{a,*}, L. Guzzi^b, J. Lynch^c

^a LURE, Bat 209D, Université Paris-Sud, 91405 Orsay, France

^b Department of Surface Chemistry and Catalysis, Institute of Isotope and Surface Chemistry, CRC HAS, P.O. Box 77, H-1525 Budapest, Hungary

^c Institut Français du Pétrole, 1 et 4 Avenue de Bois Préau, 92506 Rueil Malmaison, France

Received 25 June 2001; received in revised form 20 September 2001; accepted 2 October 2001

Abstract

This review paper will be focused on anomalous wide angle X-ray scattering (AWAXS) and more precisely on the numerous breakthroughs, which have been achieved using this technique in heterogeneous catalysis. We present some basic elements of classical X-ray diffraction (XRD) and underline the limitation of this technique when we consider the structural characterisation of nanometer scale metallic clusters supported on supports such silica, zeolite or γ -alumina. Then we introduce the theoretical formalism of the anomalous diffraction and more precisely the f' and f'' dispersive terms, including other physical processes such Compton scattering and fluorescence. A brief presentation of experimental set-ups dedicated to anomalous scattering implemented on different synchrotron radiation centres is given. We conclude with a review of the different studies already published and with some selected examples related to nanometer scale mono and bimetallic, sulfide and oxide clusters to illustrate the nature of information obtained through this technique and discuss the advantages and the limits of this approach. © 2002 Elsevier Science B.V. All rights reserved.

Keywords: Anomalous wide angle X-ray scattering (AWAXS); Heterogeneous catalysis; X-ray diffraction

1. Introduction

During recent decades, numerous academic and industrial laboratories have pursued research on nanometer scale materials, and in particular on the physics [1,2] and chemistry [3,4] of nanometer scale metallic clusters. Along with the theoretical work [5–7], this research has profited from an increasing experimental effort, which takes advantage of the growing number of synchrotron radiation cen-

tres. This approach leads to elegant experiments aimed at characterising and understanding different physical-chemical processes playing an important role not only in physics and chemistry and but in structural macromolecular biology [8].

If we turn our attention to heterogeneous catalysis [9–11], a major driving force has been importance of different environmental and industrial challenges of our modern society. Let us quote for example the reduction of NO_x in the atmosphere [12–18], the optimisation of the Fischer–Tropsch process [19–21] or the hydrogenation of hydrocarbons [22,23] which cannot be done without a fine structural description of the catalyst. It is important to underline that such materials can also

* Corresponding author. Tel.: +33-164-4680-72; fax: +33-164-4668-48.

E-mail addresses: bazin@lure.u-psud.fr (D. Bazin), guzzi@sunserv.kfki.hu (L. Guzzi), john.lynch@ifp.fr (J. Lynch).

be used in fine chemistry for different processes [24].

When classical techniques or in laboratory techniques, such as high resolution transmission electronic microscopy (HRTEM) or classical X-ray diffraction (XRD), are used to investigate nanometer scale materials these techniques reach their limit [25]. In fact, research at the cutting-edge requires the capability to perform in situ characterisation, i.e. carried out under reaction conditions [26,27]. The ultimate goal is to obtain significant structural and electronic characteristics, which can be correlated to the catalytic activity observed in a given reaction [28,29]. This explains the increasing interest of the scientific community for different synchrotron radiation related techniques. The possibilities offered by X-ray absorption spectroscopy (XAS) have been underlined [30–36]. Also, the complementary aspect of different techniques related to synchrotron radiation has already been discussed [37].

This review paper will be focused on anomalous wide angle X-ray scattering (AWAXS) and more precisely on the numerous breakthroughs, which have been achieved using this technique in heterogeneous catalysis. We present some basic elements of classical XRD and underline the limitation of this technique when we consider the structural characterisation of nanometer scale metallic clusters supported on supports such silica, zeolite or γ -alumina. Then we introduce the theoretical formalism of the anomalous diffraction and more precisely the f' and f'' dispersive terms, including other physical processes such Compton scattering and fluorescence. A brief presentation of experimental set-ups dedicated to anomalous scattering implemented on different synchrotron radiation centres is given. We conclude with a review of the different studies already published and with some selected examples related to nanometer scale mono and bimetallic, sulfide and oxide clusters to illustrate the nature of information obtained through this technique and discuss the advantages and the limits of this approach.

2. Classical X-ray diffraction

2.1. Generalities

Since the first experiment carried out using a primitive vacuum tube at the beginning of the previous

century [38], XRD has emerged to be one of the most powerful tools in almost every field of science and technology [39]. Now many books and several review articles are dedicated to the numerous methods of characterisation linked to X-ray scattering. Among them, the fundamental aspects are given in the still essential books written by Guinier [40], James [41] and more recently by Warren [42].

Concerning catalytic materials, the characterisation of such materials by X-ray methods is given almost systematically in several different books dedicated to heterogeneous catalysis [43–45]. In fact, several powerful techniques are based on X-ray photons well known now through different acronyms such SAXS for small angle X-ray scattering, WAXS for wide angle X-ray scattering as well as EDXRD for energy-dispersive XRD. Moreover, among the different articles, the review by Gallezot [46] gives a wide survey of the application of X-ray methods to identify the different phases, which constitute a catalyst. Note also that in the “Handbook of Heterogeneous Catalysis”, a section is devoted to powder diffraction as well as to particle size measurements [47].

As underlined by Bergeret [48], the powder diffraction file [49] which contains 64,000 patterns with 12,000 concerning metals and alloys in 1997 is commonly used. The XRD has been developed to study the catalyst in air at successive stages of its life (preparation, activation after reaction) and also while the chemical reaction proceeds [50]. Regarding nanometer scale metallic or non metallic cluster, we will see later the limitations of such approach.

Finally, note that using synchrotron radiation, dynamic studies can be carried out on a time scale of seconds. For example, Ciraolo et al. [51] have recently followed through an in situ X-ray powder diffraction the adsorption of hydrofluorocarbons in zeolite, the acquisition time of a scattering diagram being 5 s. An other major development is also linked to the combination of XRD with the XAS [52–62], small angle X-ray scattering [63] or other more classical methods [64] which have led to significant breakthroughs in the understanding the effect of catalyst structure on mechanisms of catalytic reaction. Finally, Walton et al. [65] have illustrated the opportunities given by EDXRD to follow the hydrothermal crystallisation of zeolites.

Before a description of the formalism associated to anomalous diffraction, we would like now to recall

the readers of some basic elements related to classical XRD. Although the theory of diffraction is the same for different types of radiation such as X-rays, electrons or neutrons, the X-ray scattering has specific interest linked to particular properties. Many of these properties were described in the original paper in which Röntgen published about their discovery [38] and include:

- The range of X-ray wavelengths: placed between the ultraviolet and γ -rays, the interval of wavelengths which is commonly considered ranges between 0.4 and 2.5 Å.
- The refractive index of X-rays is close to unity.

The ways, in which X-rays interact with matters, govern the design of sources, the nature of X-rays optics, the operation of detectors and applications. More precisely, one consider two fundamental channels: absorption (the energy of the photon is lost within the target) and the scattering processes which can be either elastic (Thomson scattering from free electrons) or inelastic (Compton scattering). The interaction of photons with nuclei is out of the X-ray energy range, between 3 and 25 keV, considered here namely. Regarding the absorption phenomena, we have already compared XAS, anomalous small angle X-ray scattering (ASAXS) and the diffraction anomalous fine structure (DAFS) with XRD in the case of nanometer scale metallic clusters [37].

The present paper is dedicated to the so-called kinematic theory of diffraction (the dynamic theory of diffraction will be not treated).

2.2. Diffraction scattering from nanometer scale metallic clusters

Regarding the nature of the materials, which is considered here, the major emphasis is given to isotropic statistically homogeneous object. More precisely, such objects consist of nanometer scale metallic clusters, which can be considered as statistically homogeneous entities (associated with given morphology and size). Also, their dispersion on a support of high specific surface leads to an isotropic orientation.

A simple way to calculate the diffraction diagram of the metallic part of a catalyst composed by a collection of nanometer scale metallic clusters with known geometry but random orientation and position is to

used the Debye scattering equation.

$$I(q) = \frac{\sum_i \sum_j f_i(q) f_j(q) \sin(qR_{ij})}{qR_{ij}} \quad (1)$$

In this equation, $I(q)$ is the angle dependent intensity from coherent scattering, q bisects the angle between the incident and scattered directions, which in turn defines the scattering plane. The sums over i and j are over all the atoms, R_{ij} being the distance between the atom i and j and f_i and f_j being the angle dependent atomic scattering factors. The energy independent part denoted also $f_0(q)$ is in fact the usual form factor related to $\rho(r)$, the electron density of the atom.

$$f_0(q) = 4\pi \int_0^\infty \rho(r) \left(\frac{\sin(qr)}{qr} \right) r^2 dr \quad (2)$$

Most of the radiation scattered at high q value is due to the electrons of inner shells of the electron cloud. Conversely, scattering of valence electrons is efficient only at low q values. For forward scattering, this parameter tends toward Z plus a relativistic correction important in the case of medium and heavy elements (Fig. 1).

From the experimental point of view, the X-ray scattering factors for neutral atoms from He to Lw

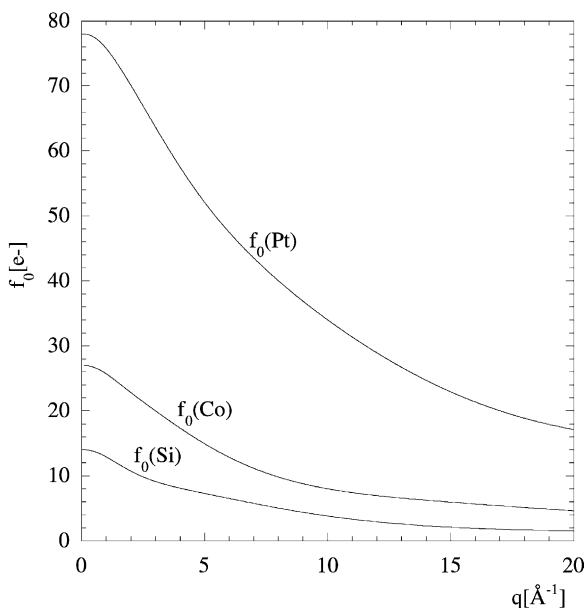


Fig. 1. $f_0(q)$ of different elements as calculated by Cromer and Liberman [95,96].

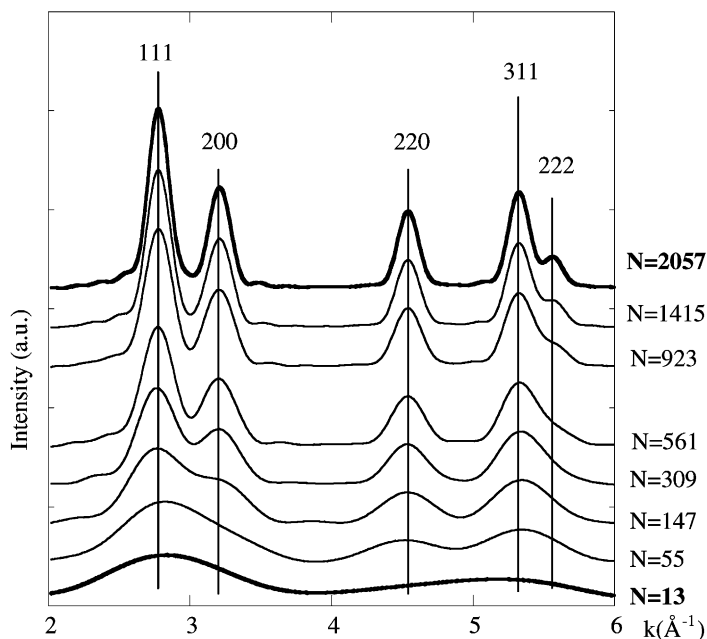


Fig. 2. Evolution of the scattering intensity vs. the size of the fcc Pt clusters.

and for most of the chemically significant ions have been computed [66–68]. As underlined by Bienenstock [69], this approach may be satisfactory for most structural studies. However, problems have been encountered in fitting the large q -scattering data to the atomic scattering factors

for heavy elements for which relativistic effects are important.

Using the Debye formulae and calculated atomic scattering factors, we have now the possibility to evaluate the diffraction intensities of very small metallic clusters. In Figs. 2 and 3, we see the numerical simula-

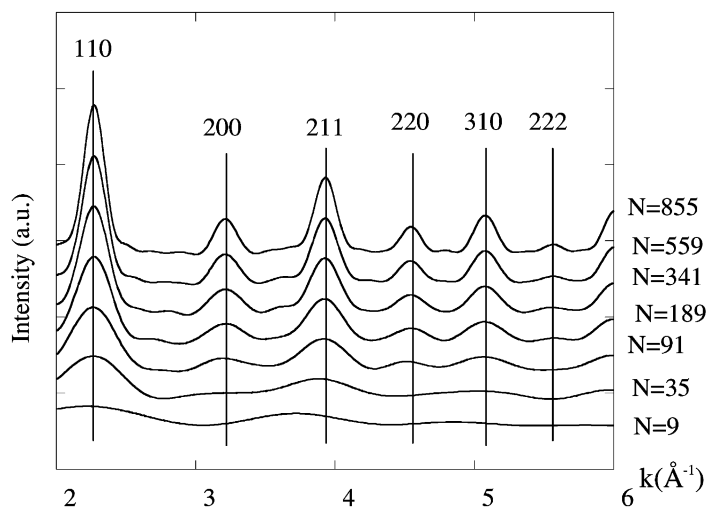


Fig. 3. Evolution of the scattering intensity versus the size of the bcc Pt clusters.

tion of the diffraction diagram obtained for nanometer scale platinum fcc or bcc clusters. We neglect here the thermal disorder as well as the Compton scattering in a first approach. In the case of platinum, this last approximation is valid since this element being a heavy element, the Compton scattering is in a small diffuse background, which increases slowly when q increases.

As pointed by Gallezot and coworkers [70,71], the different diffraction diagrams (Figs. 2 and 3) clearly show that even for extremely small clusters, the Bragg diffraction peaks of an fcc network are clearly visible. Thus, the nature of the network can be directly determined even for very small clusters.

Secondly, although the classical Scherrer formula cannot be used to determine the size of the cluster because the peaks are overlapped, the splitting between the peaks can be extremely sensitive to the size of the clusters allowing an indirect measure of the cluster size. Thus, the separation between the (1 1 1) and the (2 0 0) peaks can be used as a determination of the size if the number of atoms inside the cluster is <1000 .

Finally, such simple calculations underline the fact that the conventional practice of phase identification as introduced before is no longer valid for nanometer scale metallic clusters. In fact, at this point, another method, the Debye function analysis method as developed by Gnutzmann and Vogel [72] has to be used. This method is based on a simulation using a linear combination of ab initio calculated diffraction diagrams obtained through the Debye equation. Note that using this original approach, the information regarding the size and morphology distribution has been obtained in the case of a Pt/SiO₂ catalyst namely the standard catalyst EUROPT-1 [72,73], a surfactant-stabilized Pt–Ru alloy system [74] as well as in the case of Au₅₅ organic complexes [75].

2.3. Some limitations of X-ray diffraction

If we compare XRD versus neutron diffraction, the first limitation is linked to the atomic scattering factor $f_0(q)$ which decrease rapidly with q . Fig. 1 which displays the atomic scattering factors of different elements namely Pt, Co, Si illustrates this behaviour. This originates from the fact that X-ray scatters is the electrons rather than nuclei. Note that this interaction process leads to a modulation of the atomic factor $f_0(q)$ due to the atom's chemical state.

A further problem arises from inelastic processes, i.e. Compton scattering and fluorescence emission. The Compton scattering [76–78], contribution has to be removed from the total scattering. It corresponds to a distribution of energies at each scattering angle 2θ which has a maximum for an energy loss $\Delta E = E - E_0$ at

$$\Delta E = \left(\frac{E_0^2}{mc^2} \right) (1 - \cos 2\theta) \quad (3)$$

where E_0 is the initial photon energy.

Among the different methods, which have been developed to remove this parasite signal, the most common is the use of a crystal monochromator [79] placed just before the detector.

In a first approximation, the fluorescence can be treated as a smooth background and eliminated by background fitting procedures. A more elegant approach based on a measurement of the K_α/K_β fluorescent intensities ratio above the absorption edge has been given by Raoux and coworkers [80–84].

2.4. Diffraction scattering from supported nanometer scale metallic clusters

In the case of real catalysts such as nanometer scale metallic clusters supported on high surface metal oxides, the major difficulty is linked to the low loading of metal ($<1\%$ in weight). At this point, we can distinguish basically two cases.

A configuration in which the contribution coming from the support in the diffraction diagram is similar to a small diffuse background which decreases slowly when q increases. This assumption is valid in some particular cases such as amorphous silica for example. In this case, the procedure generally followed is to obtain careful diffraction patterns for the sample of interest and for the support material alone. The contribution of the support is then subtracted out to yield the diffraction pattern of interest.

Nevertheless, for numerous supports, several diffraction peaks are present in the diffraction diagram. This is the case for γ -alumina, TiO₂ or zeolite for example. In this case, a more elegant approach to remove the contribution of the support is given by anomalous diffraction. Before the introduction of the different physical parameters which are linked to this

technique, we would like to make some comments about this original approach taking as an example the case of nanometer scale platinum particles supported on alumina.

For this system, we can distinguish two contributions in the diffraction diagram. The first contribution originates from the support, i.e. the alumina, the second resulting from the platinum. A first diffraction diagram is collected as in classical XRD diffraction at one photon energy. If we are able to collect a second diagram (at a different photon energy) for which the contribution originates from the support is exactly the same, but for which the contribution resulting from platinum particles is different, we will be able through a simple subtraction between the two diffraction diagrams to obtain a contribution resulting from the platinum particles alone. To do so, we will use the fact that the atomic factor of aluminium and oxygen are constants for these two energies, while the atomic factor of platinum is modified.

As we have seen in equation [2], the atomic factor $f_0(q)$ is independent of the photon energy. But as we will see in the next section, the atomic factor contains two other terms $f'(E)$ and $f''(E)$ which are photon energy dependent.

3. Anomalous wide angle X-ray scattering

3.1. Generalities

The technique (see for more details on the theoretical background [85–90]) is based on the energy dependence of the atomic scattering factor $f(q, E)$ near to the absorption edge. This parameter is expressed in electron units as

$$f(q, E) = f_0(q) + f'(E) + if''(E) \quad (4)$$

where q bisects the angle between the incident and scattered directions which in turn define the scattering plane, $f(q, E)$ gives the amplitude of the radiation coherently scattered by a single atom. This physical parameter is composed of an energy independent part $f_0(q)$ as discussed in the previous section. In order to discuss the anomalous aspect of this technique we now consider the real and imaginary energy dependent corrections $f'(E)$ and $f''(E)$. In fact, these quantities are the sum of different order tensors. Nevertheless,

even though the representation of f' and f'' as scalars is generally invalid [91], this simplification leads only to small errors.

3.2. The terms f' and f''

The real and imaginary energy dependent corrections originate mostly from the tightly bound inner electrons. Thus, these terms vary rapidly when the photon energy is close to that needed to eject such electrons leading to a competition process between absorption and diffraction. The imaginary part can be determined directly from a measurement of the photoelectric absorption with the optical theorem:

$$f''(q, E) = \frac{mcE\sigma(E)}{2he^2} \quad (5)$$

where $\sigma(E)$ is the atomic cross-section as a function of incident X-ray energy, E , m the electronic mass, e its charge, h is Planck's constant and c the speed of light.

We observe a jump for f'' which corresponds to the photoabsorption process. The first theoretical calculations were performed by Höln [92,93], Sasaki [94] and by Cromer and Liberman [95,96]. This jump is abrupt as we can see in Fig. 4 which displays the dispersive f' and f'' terms for platinum. Finally, we can obtain

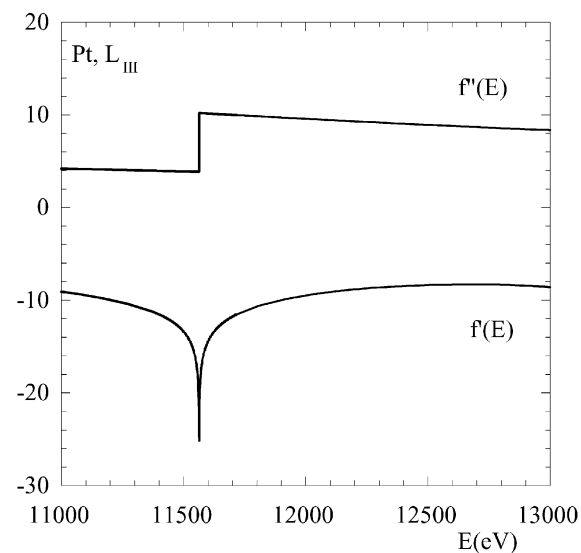


Fig. 4. $f'(E)$ and $f''(E)$ as calculated by Sasaki for platinum near the L_{III} absorption edge.

the other term namely $f'(E)$ either through experimental data [97–99] or through the Kramers–Kronig dispersion relationship which links f' and f'' [100].

$$f'(E) = \frac{2}{\pi} P \int_0^{\infty} \frac{\varepsilon f''(E)}{\varepsilon^2 - E^2} d\varepsilon \quad (6)$$

P denotes the Cauchy principle value of the integral. Due to the presence of an absorption edge, a significant decrease in $f'(E)$ is observed, peaking in magnitude at the edge energy. In the case of platinum, the variation of f' is equal to $16e^-$ while the maximum value of f_0 is $72e^-$ (Fig. 4). We will see that this relatively small variation of f' implies a careful measurement of the scattering intensity.

Note also that f'' (and thus f') depends on the ionic state and the chemical environment of each diffracting species. In the case of oxide materials, large “white lines” are present at the edges in the absorption spectra.

3.3. Anomalous diffraction scattering from supported nanometer scale metallic cluster

As we have seen in the previous section, the ultimate goal is to extract a diffraction signal coming only from the supported metallic phase. In the case of nanometer scale platinum particles supported on alumina, this goal implies that we have to choose the photon energy close to an absorption edge of platinum. More precisely, the L absorption edges which have absorption energy close to 10 keV, constitute very good candidates. Thus, the atomic factor of aluminium and oxygen can be considered as constant, the photoabsorption energy of these elements being very low.

There is now a simple question. How to choose these two energies? As we have pointed out, the term f'' varies significantly if we choose these two photon energies above and below the absorption energy of the platinum. An other choice is to consider not $f''(E)$, but $f'(E)$. In this case, we can choose the first energy far below the absorption edge and the other one close to the absorption edge. We have to evaluate these two choices by introducing the fact that $f(q) = f_0(q) + f'(E) + f''(E)$ in the Debye equation.

In the case of monometallic clusters, the difference between the two diffraction diagrams is similar to the

diffraction intensity as shown in the Debye equation [1].

$$\begin{aligned} \Delta I(q) &= \frac{\sum_i \sum_j \Delta f_i(q) \Delta f_j(q) \sin(qR_{ij})}{qR_{ij}} \\ &= \frac{(\Delta f(q))^2 \sum_i \sum_j \sin(qR_{ij})}{qR_{ij}} \end{aligned} \quad (7)$$

$$(\Delta f(q))^2 = ((f_0(q) + f'(E_1))^2 - f''(E_1)^2)((f_0(q) + f'(E_2))^2 - f''(E_2)^2) \quad (8)$$

$$\begin{aligned} (\Delta f(q))^2 &= 2f_0(q)(f'(E_1) - f'(E_2)) + (f'(E_1)^2 \\ &\quad - f'(E_2)^2) - (f''(E_1)^2 - f''(E_2)^2) \end{aligned} \quad (9)$$

For large value of q , the magnitude of $f_0(q)$ is more important than that of the f' and f'' terms. Thus, the dominant term here is $2f_0(q)(f'(E_1) - f'(E_2))$. This implies that variation of $f'(E)$ is preferred to that of $f''(E)$ if we want to optimise the value of the difference. Moreover, if we consider the variation of $f''(E)$, i.e. a photon energy above the absorption energy, we add a supplementary signal in the detector coming from fluorescence processes. Thus, the conclusion is quite clear. We have to consider the term $f'(E)$. For $f_0(q)$, we used the Cromer and Liberman parameters (63) and the values of f' and f'' for platinum according to the SASAKI tables ($E = 11450$ eV, $f' = -12.25$, $f'' = 3.93$; $E = 11540$ eV, $f' = -15.35$, $f'' = 3.88$). As we can see on Fig. 5 the weak amplitude of the difference induced by the small variation of $f'(E)$ (versus the value of $f_0(q)$) implies a careful measurement of the scattering intensity.

Thus, as pointed out by Lengeler [101], an experimental measurement of f'' through a conventional EXAFS experiment and a numerical evaluation of f' using the Kramers–Kronig dispersion relationship must be performed. Fig. 6 shows the result for the f' and f'' term related to platinum atoms in their metallic state (note the low amplitude of the white line intensity).

3.4. Anomalous diffraction scattering from supported nanometer scale bimetallic clusters

Bimetallic systems are more and more the subject of AWAXS studies. In a previous work simple calculations showed that it was possible to determine the distribution of the metals inside the crystallite [102,103].

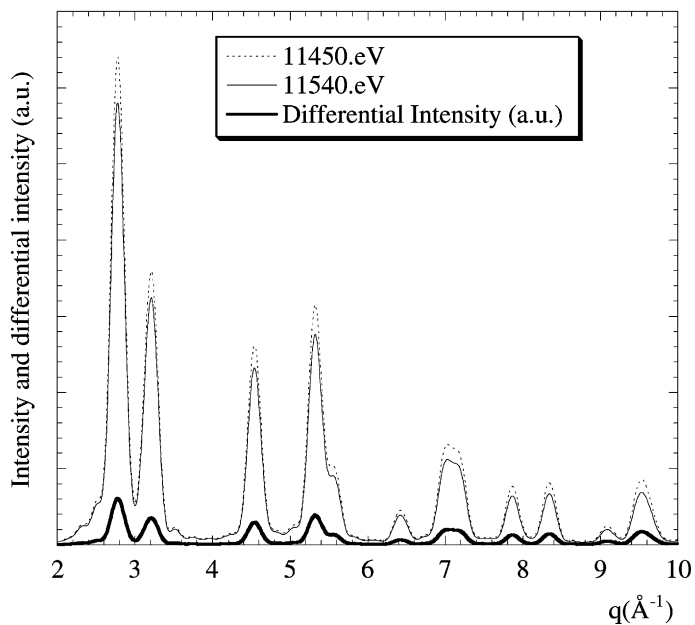


Fig. 5. Comparison between the diffraction intensity and the differential intensity for a platinum cluster containing 1415 atoms.

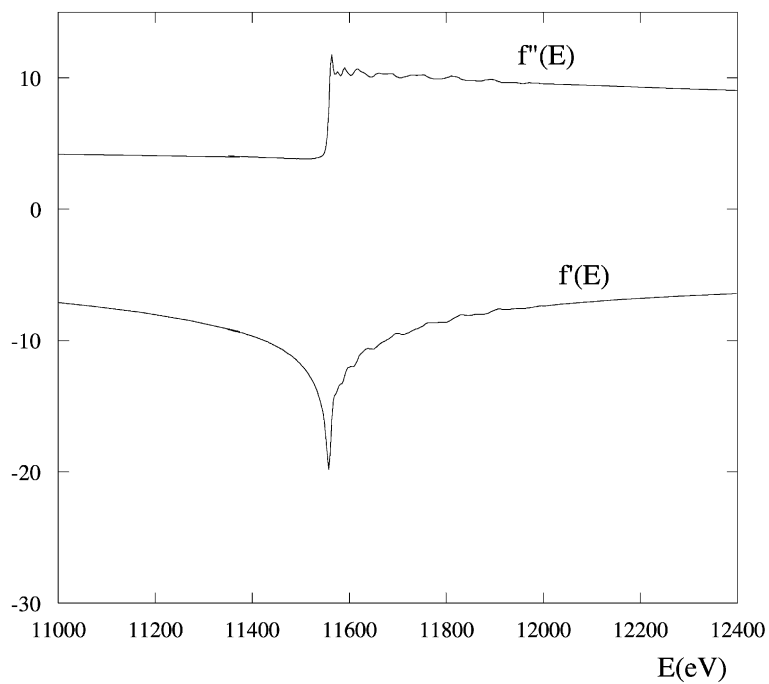


Fig. 6. $f''(E)$ in which the EXAFS data have been inserted and $f'(E)$ as calculated through the Kramers–Kronig relationship.

This is particularly important in the case of bimetallic systems for which the two metals are close in the periodic table. For such bimetallic systems, EXAFS spectroscopy cannot give structural evidence regarding the existence of bimetallic clusters. This is due to the similarity of the backscattering amplitude and phase of the two metals. Such major information is available using the anomalous diffraction technique.

We take as an example, we can take the Pd–Rh system, which can be used in diastereo-selective hydrogenation of 4-phosphono-methyl-2-pyridine carboxylic acid [104]. For this particular system, we take an approach we have previously developed for the bimetallic Pt–Mo system [103]. Thus, we calculate the differential intensity in the case of following clusters:

- *cluster A*: a statistical distribution of the two metals inside the cluster;
- *cluster B*: a preferential distribution of the two metals: palladium atoms are at the surface and rhodium atoms at the core (147 atoms of palladium define the core and 162 atoms of rhodium define the surface).

For $f_0(q)$, we used the Cromer and Liberman parameters [95,96] and the values of f' and f'' for each element (Fig. 7) was obtained through [94,105].

For cluster A (Fig. 8), the differential intensity, i.e. the subtraction between the two classical diffraction diagrams named also the WPSFs (weighted sum of

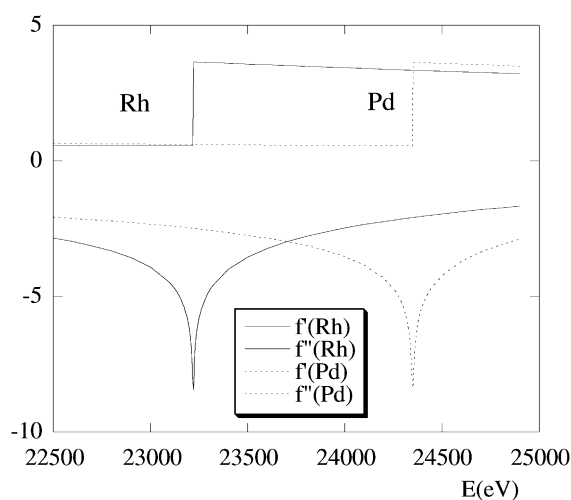


Fig. 7. $f'(E)$ and $f''(E)$ as evaluated by for rhodium and palladium.

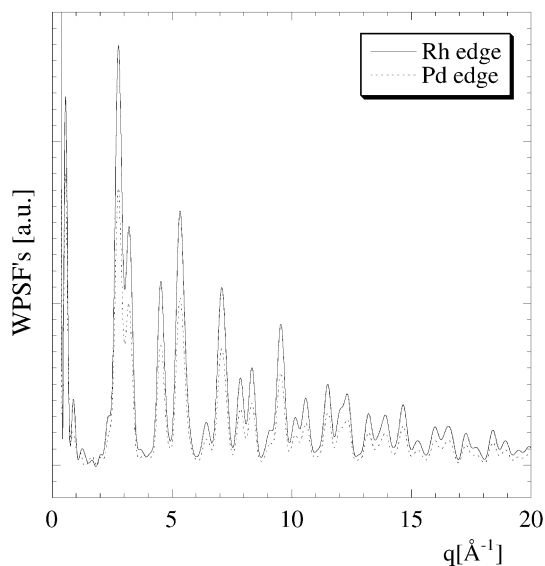


Fig. 8. WPSFs calculated for a statistical distribution of palladium and rhodium atoms inside the metallic cluster.

partial structure factors) at the Pd and Rh edges are basically the same. At the opposite, for cluster B (Fig. 9), the splitting between the (1 1 1) and (2 0 0) peaks is lesser well defined for the WPSFs at the Pd edge than those at the Rh edge. As previously discussed

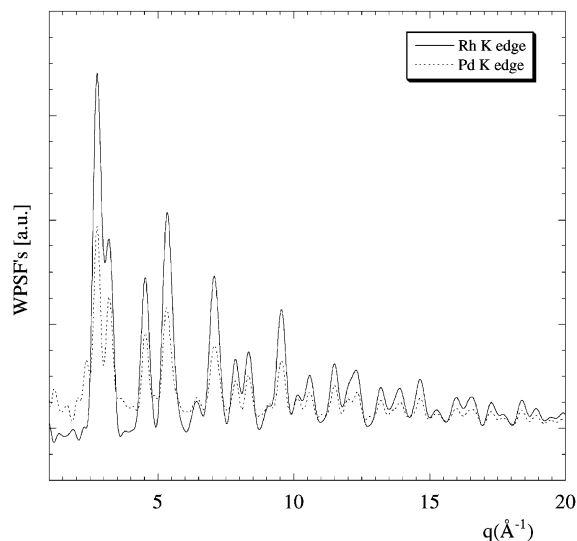


Fig. 9. WPSFs calculated for a preferential distribution of the two metals inside the metallic cluster.

[102,103], surface atoms associated with a diffraction peak split the peak to a greater extent than the core atoms. This behaviour can be easily understood. The splitting is directly related to the size or, more precisely, is correlated with the longer distances in the cluster. This maximum distance is obviously obtained for surface atoms, which are all located on the outer surface. When we calculate the WPSFs by removing the surface atoms, we also remove this distance and, thus, the maximum distance in the calculation is less.

Also, previous calculations performed on Pt–Mo clusters have shown that the AWAXS technique offers the possibility to locate the surface atoms. To illustrate this possibility, we have considered a large cluster of 561 platinum atoms on which we put Mo atoms either on a (1 1 1) face (cluster F $\text{Pt}_{561}\text{--Mo}_{80}$) or on a 100 face (cluster G $\text{Pt}_{561}\text{--Mo}_{150}$). If we calculate the WPSFs associated with this cluster it is clear that the width of the (200) peak is broader when Mo atoms are put on a (1 1 1) face (Fig. 10). Thus, information on the distribution of Mo at the surface of the cluster

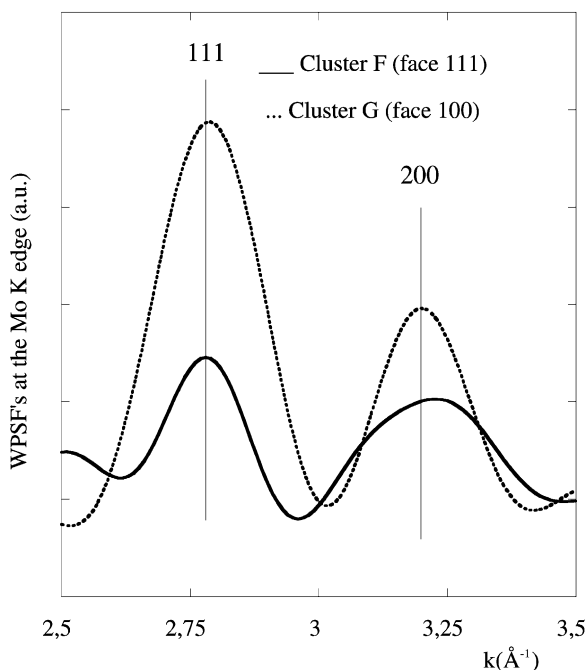


Fig. 10. WPSF's associated with cluster F and cluster G (Mo K edge).

is also available using AWAXS. Moreover, from an experimental point of view, calculation of the structure of the WPSFs shows that only a small part of the spectra need to be measured and thus this approach can significantly decrease the acquisition time devoted to such study.

4. Experimental devices for AWAXS experiments

Now, we would like to give a brief presentation of experimental set-ups implemented on different synchrotron radiation centres and on which heterogeneous catalysts have been characterised.

One of the first studies was performed by Georgopoulos and Cohen [106] at the Cornell high energy synchrotron source (CHESS) using a monochromator with a flat Si(1 1 1) crystal followed by a triangular slotted, sagittally focused Si(1 1 1). Each measurement lasted approximately 1.5 h. All measurements were performed for fixed monitor count to eliminate variation in incident beam intensity. Among the different experimental difficulties, was the lack of a mirror to eliminate high order reflections, which were intense, the electron energy being 5.5 GeV beam. Another difficulties resulted from the instability of the electron orbit as a function of time. Such process leads to a modulation of the harmonic component of the beam. Ion chambers filed with nitrogen (respectively xenon) were used to measure initial intensity (respectively the diffracted intensity).

A significant improvement of the signal to noise ratio was obtained by Liang et al. [107] at Stanford Synchrotron Radiation Laboratory (SSRL). This time, experiments were performed on a wiggler beam line (beam line IV.3) and not a bending magnet. This insertion device is able to deliver much more photons. Also, a Si(2 2 0) double-crystal incident beam monochromator with proper detuning has been used to limit harmonic contamination of the incident beam. Finally, the incident intensity I_0 was monitored with a scintillation detector and the scattered intensity I was measured with an intrinsic Ge detector. The sample was placed on a two-circle diffractometer in the symmetrical reflection mode.

Finally, the presence of mirror constitutes another possibility to increase the quality of the data. This is the case of the beamline 1-BM/SRI-CAT implemented

at the advanced photon source (APS) at Argonne National Laboratory. The monochromator is a Si(1 1 1) PSL double-crystal monochromator with a sagittal focus for which the estimated resolution ($\Delta E/E$) is equal to 1.5×10^{-4} . A vertical focusing mirror at 45.5 m from the source is positioned after the monochromator. Finally, a variety of detectors is available such as NaI scintillation counters, ionisation chambers, Si(Li) and Ge energy dispersive detectors, CCDs as well as image plates.

More recently, Favre-Nicolin et al. [108] have reported AWAXS experiment carried out on the French CRG beam line D2AM at the European synchrotron radiation facility (ESRF). This beam line is installed at the output of a bending magnet. The optics consists of a double-crystal monochromator located between two mirrors. This arrangement provides a fixed-exit monochromatic beam and maintains the focal spot constant during energy tuning. Finally, a heavy load 2 + 4-circle diffractometer is set-up in a large vacuum vessel to perform scattering experiments either in the vertical or horizontal scattering planes. An analyser assembly is mounted on the detector arm to provide high Q resolution or data acquisition free of inelastic scattering contributions.

At the ESRF also, another beam line ID11 is dedicated to diffraction experiments in the area of materials science. The main optical elements are a 1 m long Pt-coated Si pre-mirror, which is adaptive to cope with the high heat load, a double crystal monochromator, and a second 1.2 m long Pt-coated mirror. Other components are an attenuator system in front of the first mirror (six sets of three attenuators) and water-cooled slit systems. The monochromatic beam is 20 cm below the orbital plane, and the reflected white beam 17 cm above the plane, excluding high energy Bremsstrahlung background. Focusing is done in the horizontal plane by a sagittal bender for the second monochromator crystal, and in the vertical plane by the second mirror. Sagittal focusing can currently be achieved up to 30 keV. To avoid thermal distortions of the first monochromator crystal, liquid nitrogen cooling is employed via a closed-loop cooler system with a flow of 25 l/min. The monochromator is currently operated with two Si(1 1 1) crystals. Thus, the wavelength is tunable in the energy range 7–100 keV with an energy resolution close to $\Delta E/E = 10^{-4}$ up to 40 keV, making it suitable for anomalous disper-

sion around X-ray absorption edges. Recently, a new heavy duty, high precision eight-circle kappa diffractometer has been implemented. Note that the sphere of confusion has been measured at 14 μm and the sample arm can take a load of 5 kg.

Finally, the Italian Collaborating Research Group GILDA at ESRF is a general purpose beam line using a bending magnet source. The XAS as well as XRD is used on the beam line in the energy range 5–80 keV. A high energy resolution is ensured by using Si(3 1 1) and Si(5 1 1) crystals. Among the different possibilities given by this experimental device, one set-up, in 1:1 focal geometry, is dedicated to X-ray scattering and diffraction. It is equipped with a two circle diffractometer with an angular step of 0.28 arcsec and a reproducibility of 2 arcsec. Crystal analysers, solid-state detectors and scintillators are used to perform anomalous scattering on amorphous materials, and powder diffraction with an instrumental angular resolution $<0.01^\circ$. The recent installation of an image plate detector has permitted the development of an apparatus for time-resolved powder diffraction.

At LURE (Orsay), the original work in heterogeneous catalysis was performed by the group of Raoux and coworkers [80–84]. Such diffraction experiments can be performed using the synchrotron radiation from the DCI storage ring running at 1.85 GeV with a typical current of 300 mA and a time life of 200 h. The diffraction diagrams can be collected either on the W31 (or the W22) wiggler beamline [109].

The W31 Wiggler beamline (Fig. 11) is equipped with a Si(1 1 1) double crystal monochromator. Energy calibration is made by recording the fluorescence of the sample and compare to X-ray absorption spectrum measurements in transmission. An entrance slit of 2 mm \times 4 mm limits the incident beam which is monitored by an ionisation detector. The scattered beam is collected by a 12 pixel solid-state detector which allows simultaneous collection of 12 spectra for each angular scan. This experimental improvement compared to the classic NaI scintillation detector yields, in about 8 h of measurements, differential intensities with a low noise level of a few percent even for a low concentration species [110,111].

Finally, H10 is a new beamline (Fig. 12) for materials studies [112] implemented at DCI based on the complementary aspect of different techniques

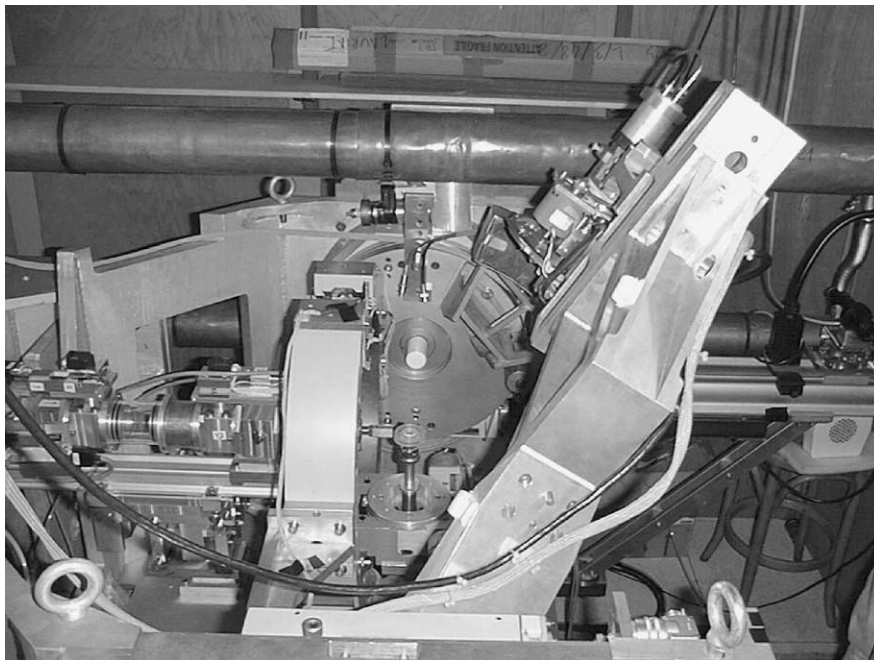


Fig. 11. The goniometer of the W31 Beamline.

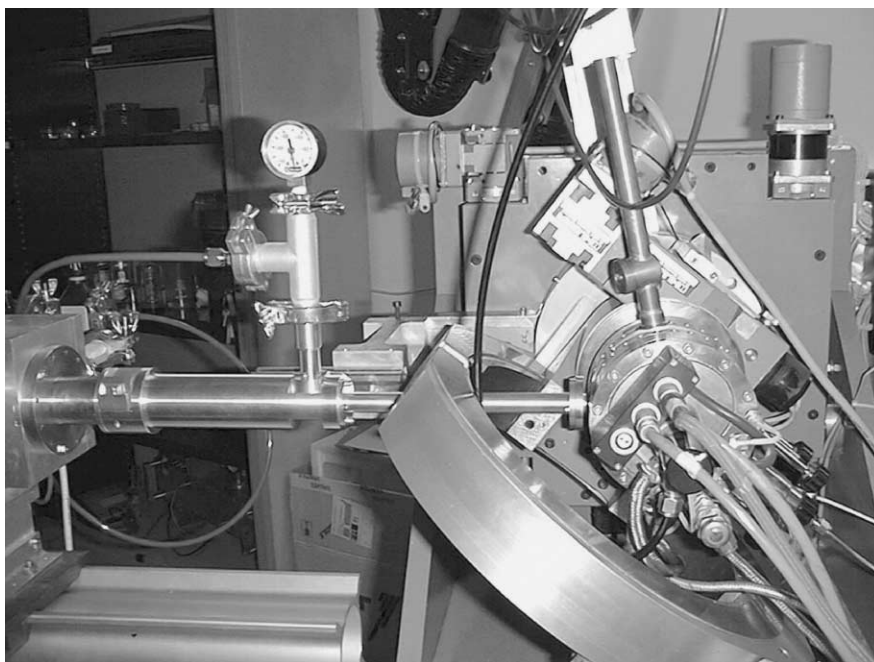


Fig. 12. The goniometer of the H10 Beamline equipped with an Parr reactor.

specific to synchrotron radiation [37]. The XRD and XAS are both feasible, in the 4–20 keV range. The XAS as well as XRD are carried out in the monochromatic mode, using a fixed exit Si(1 1 1) double crystal monochromator. Although XAS and XRD can not be measured exactly at the same time, the possibility to do both measurement consecutively without changing the set-up is an advantage when the samples are not very uniform or when it is important that the physical parameters, or the atmosphere are identical. This is mainly a concern when carrying out experiments on “real” materials, in particular using extreme conditions.

The beamline is separated from the storage ring by a 150 μm thick Be window. A 1.5 μm resolution beam position monitor is used for the storage ring feedback, and molybdenum water-cooled slits delimit the white beam before the optical hutch. The white X-ray beam is collimated by the first mirror placed before the monochromator. The monochromatic beam is then focused in the horizontal plane by the monochromator second crystal and in the vertical plane by a second mirror. Both mirrors are coated with rhodium and ensure the rejection of the monochromator harmonics.

Experiments are mostly carried out on a 4+2-circles Huber diffractometer, moved by step motors (resolution 0.001°). Either a NaI:Tl scintillator detector or one of several gas filled position sensitive detectors, in particular a CPS 120 Inel detector, are used for diffraction measurements.

5. The analysis procedure

For supported metallic catalysts, Ratnasamy and coworkers [113,114] have shown that the method of direct intensity calculation and the radial distribution method are rather complementary to each other.

5.1. The method of direct intensity calculation

For the first method and in the case of classical XRD, the procedure to analyse diffraction intensity of nanometer scale metallic cluster can be the following. The first step is to set-up plausible models. Such structural hypotheses are made by building files containing

the Cartesian co-ordinates of the atoms which are involved in the cluster. For practical reasons, the format of the input file of our program (program Build [37]) is the same as the input file of the FeFF program, which is used to simulate the X-ray absorption spectra. Then the diffraction intensity is calculated through the Debye formulae) using the Cromer and Liberman tables [95,96] for $f_0(q)$. Such calculations can be done for a family of clusters having different arrangements (bcc, fcc icosahedron) and morphologies (for fcc clusters: cuboctahedron and Wulff polyhedron). A refinement performed on a linear combination of these diffraction intensities, following the Debye method, is then done to simulate the experimental data.

In case of anomalous scattering, a similar approach can be performed. Now, for each structural hypothesis, the differential intensity is calculated through the Debye formula using the Cromer and Liberman tables for $f_0(q)$ and the Sasaki tables [94]

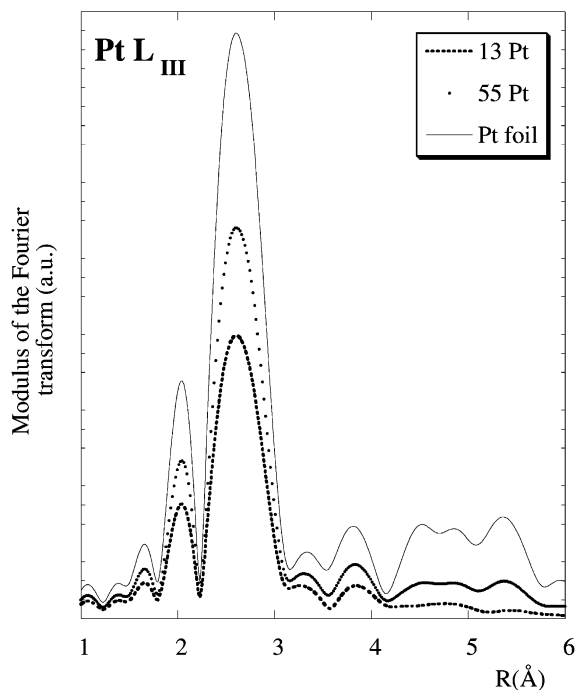


Fig. 13. Modules of the Fourier transform uncorrected from phase shift associated with clusters of 13 atoms (13 Pt, dashes) and 55 atoms (55 Pt, dots) of platinum compared to the modulus of a platinum foil (line).

for $f'(E)$ and $f''(E)$. The model is then refined until a satisfactory agreement is reached between a linear combination of the differential intensities and the experimental data. This synthetic approach means that, at contrary of XAS analysis, size distribution is here included from the beginning of data treatment.

5.2. The radial distribution method

Considering Fourier transform, it is convenient to introduce the partial structure factor $S_{mn}(q)$, q being the wave vector. $S_{mn}(q)$ is related to the pair distribution function by the following relation:

$$S_{mn}(q) = \frac{4\pi}{q} \int_0^{\infty} (\rho_{mn}(r) - \rho_{n0})r \sin(qr) dr \quad (6)$$

where $\rho_{mn}(r)$ is the pair distribution function (i.e. the density of atoms of type n at a distance r from an atom

of type m) and ρ_{n0} is the average atomic density of atoms of type n in the sample. We have then

$$I(q) = \sum_n \sum_m x_m f_m(q) f_n(q) S_{mn}(q) \quad (7)$$

where x_m is the atomic fraction of atoms of type m .

In the case of nanometer scale metallic cluster, we can discuss the sensitivity of the absorption and diffraction techniques [37] through a simple comparison between the Fourier transform of the EXAFS modulations (Fig. 13) and the radial distribution function obtained from diffraction data (Fig. 14). Note that the two Fourier transform are performed over a similar k range.

The comparison shows clearly that the diffraction technique is better than the absorption spectroscopy for the determination of the local order after the first shell. This is due obviously to the fact that the low k range of the absorption spectrum is dominated by multiple scattering processes which lead to a loss of information in the high R range.

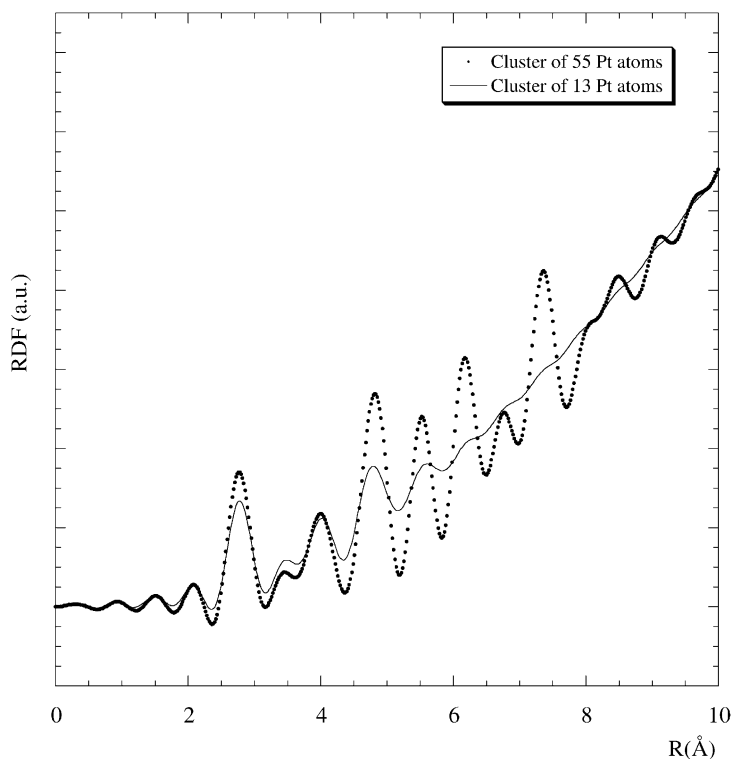


Fig. 14. Radial distribution function (RDF) calculated for a cluster of 13 atoms (line) and a cluster of 55 atoms (dots) of platinum.

6. Survey of the use of AWAXS in heterogeneous catalysis

6.1. Monometallic catalytic system

6.1.1. Monometallic platinum supported systems

As pointed out previously in the experimental section, one of the first works dedicated to heterogeneous catalysis was performed by Georgopoulos and Cohen [106]. The anomalous scattering experiments were conducted at the Cornell high energy synchrotron radiation source (CHESS) on three supported platinum catalysts, two of platinum on silica gel and one of platinum supported on alumina. The first sample contains large particles and the support scattering is smooth. As discussed in Section 2.4, the diffraction peaks related to the platinum are clearly visible. The authors note one key advantage of the anomalous scattering versus classical diffraction. The high angle peaks in the differential intensity are not strongly attenuated versus 2θ as in each of the two classical diffraction diagrams. As pointed in equation [9], the differential intensity is roughly proportional to $f_0(q)$:

$$(\Delta f(q))^2 = 2f_0(q)(f'(E_1) - f'(E_2)) + (f'(E_1)^2 - f'(E_2)^2) - (f''(E_1)^2 - f''(E_2)^2)$$

rather than $f_0(q)^2$. Such behaviour allows thus a more fine analysis of the structural characteristics of the supported metallic phase of the catalyst.

Another interesting remark is made regarding small metallic particles, i.e. having a diameter of 12–15 Å. For such samples, it is not possible to remove the signal coming from the support accurately through the conventional method especially near sharp features of the support scattering. This is mainly due to the fact that determination of particle size distribution is very sensitive to the tails of the profiles leading rapidly to significant errors. Finally, the authors underlined that this technique is suitable for examining catalysts under working conditions and is superior to XAS determination of particle morphology and size distribution.

Liang et al. [107] have also successfully separated the diffuse diffraction pattern associated with small Pt particles from the strong scattering of crystalline η -Al₂O₃ as well as amorphous SiO₂ supports. In the case of the 2.5 wt. Pt/SiO₂, the diffraction from Pt, exhibited as sharp Bragg peaks superimposes with the

diffuse scattering from the amorphous SiO₂ support. Then the authors estimate the average crystallite size of the Pt particle through a measurement of the widths of the peaks present in the differential intensity. The study of the two catalysts corresponding to the alumina support is very exciting due to the high dispersion of the metallic phase (around 70–80%). When the two structural properties of these catalysts, namely, the support associated to well-defined diffraction peaks on top of which there are very small metallic particles deposited, it is definitely not possible to use classical diffraction. We have to perform anomalous diffraction experiments to obtain structural information on the metallic phase. This approach allows the authors to give clear structural evidence that the Pt particles are amorphous in the air exposed case and become nano-crystalline after hydrogen reduction. More precisely, they calculated the real space radial distribution function by Fourier transformation and showed that the network of the Pt particle was face centred cubic. Finally, they also report the advantages of this technique over EXAFS in revealing long-range structure.

In the work of Ma et al. [115], XRD diagrams have been collected for a supported Pt catalyst: the monometallic system Pt/ZSM-5. The sample was prepared by ion exchange using [Pt(NH₃)₄]²⁺ as a precursor. It appears that for the as prepared sample all Pt atoms exist in the tetramine complex.

Shamkov et al. [116] have published an extensive study on the structure and phase composition of EuroPt-1 catalyst (6.3 wt. %/SiO₂). The goal of the study was to obtain structural information on a metal–support interaction. A precise analysis of interatomic distances present in the partial radial distribution function (RDF) has been performed. Approximation of RDF peaks by Gauss profiles gives direct structural evidence of two phases, the metal platinum and platinum oxide PtO and thus no metal–support interaction has been detected.

AWAXS and EXAFS experiments were also performed by Serimaa et al. [117] with synchrotron radiation in the vicinity of the Pt L_{III} absorption edge to study the structure of amorphous platinum uridine green sulfate. Earlier studies performed on this complex suggested the existence of either a polymeric mixture [118] or homogeneous polynuclear Pt complexes [119]. The refinement of the experimental data gave the shortest Pt–Pt distance of Pt-uridine green

sulfate of 3 Å with a coordination number of about 1/2. The values of these structural parameters agree with a mixture model where the major components are mono and binuclear Pt complexes. The authors encourage the use of the AWAXS method to solve a specific partial structure factor of a multicomponent system even if the sample contains only one element with a suitable absorption edge for the measurement.

6.1.2. Monometallic cobalt supported systems

In the case of cobalt catalysts for the Fischer–Tropsch reaction, with metal particles of several tens of nanometers in diameter, different supports have been compared. Various conclusions have been drawn as to the effect of the support on the activity and selectivity of these catalysts. Although in a study by Bartholomew [120] the catalytic activity of supported cobalt decreased in the sequence of $\text{Co}/\text{TiO}_2 > \text{Co}/\text{SiO}_2 > \text{Co}/\text{Al}_2\text{O}_3$. Bessel [121] obtained a higher activity for alumina support than for silica while Iglesia et al. [122] found no effect on changing the support. Fischer–Tropsch catalysts [123] were prepared by incipient wetness impregnation of TiO_2 , SiO_2 and Al_2O_3 using aqueous solutions of cobalt nitrate. The samples were dried in air and calcined at 573 K before characterisation. The XRD showed that the only crystalline form of cobalt present was Co_3O_4 and the corresponding particle sizes were determined by line broadening. Details of cobalt loading, specific surface area and Co_3O_4 particle size are given in Table 1.

The XRD studies of Co/SiO_2 and $\text{Co}/\text{Al}_2\text{O}_3$ were carried out using $\text{Cu K}\alpha$ radiation on a Siemens D501 θ – 2θ powder diffractometer equipped with an Parr reactor adapted to allow Fischer–Tropsch reactions to be carried out [124]. Reduction studies were carried out under hydrogen flow, ramping the temperature up to the desired value at 5 K/min then keeping the temperature stable during XRD analysis (4 h). The silica support is amorphous allowing the XRD pattern due to

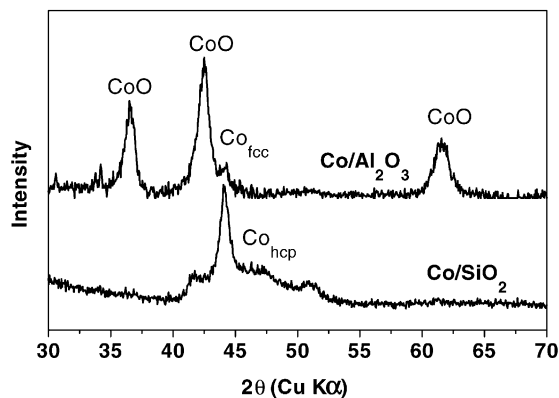


Fig. 15. In situ XRD patterns of Co/SiO_2 and $\text{Co}/\text{Al}_2\text{O}_3$ at 673 K under H_2 .

cobalt phases to be clearly identified. For the poorly crystallised alumina sample an XRD pattern of the support without cobalt was subtracted after normalisation (Fig. 15). In the case of Co/TiO_2 , the presence of many sharp lines from the support (rutile and anatase forms) prevents the cobalt phases from being correctly analysed (Fig. 16). This sample was studied using the anomalous diffraction effect at LURE (Orsay) on the H10 beam line. The difference pattern of XRD data recorded at energies far from (7614 eV) and close to (7715 eV) the cobalt K edge allowed the cobalt phases to be isolated.

Reduction of the Co_3O_4 phase under H_2 proceeds via the formation of CoO to the formation of metallic cobalt. The XRD pattern after reduction at 773 K shows the presence of both fcc and hcp form of cobalt. Comparing the XRD patterns of the Co/SiO_2 and $\text{Co}/\text{Al}_2\text{O}_3$ catalysts at 673 K shows that the degree of reduction differs for the different supports. The silica supported catalyst is more strongly reduced at 673 K than the $\text{Co}/\text{Al}_2\text{O}_3$ sample (Fig. 15). This is in agreement with temperature programmed reduction studies showing that Co/SiO_2 is fully reduced at

Table 1
Characteristics of the cobalt catalysts

Catalyst	Co loading (wt.%)	Specific surface area (m^2/g)	Co_3O_4 particle size (nm)
Co/TiO_2	11.3	16	75
Co/SiO_2	13.0	460	14
$\text{Co}/\text{Al}_2\text{O}_3$	10.5	180	20

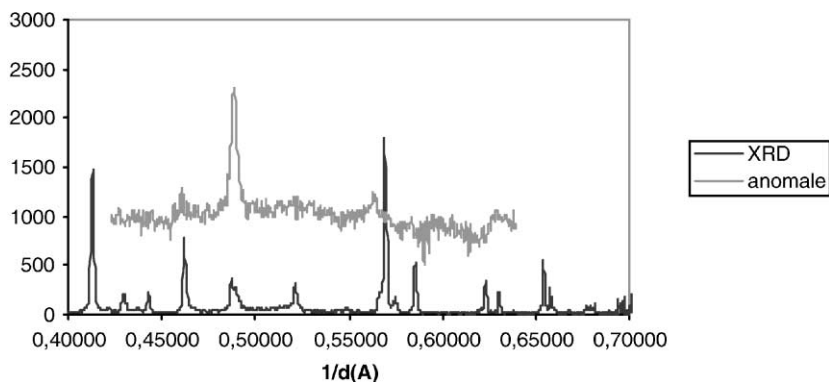


Fig. 16. In situ XRD pattern and differential intensity of Co/TiO₂ at 673 K under H₂.

this temperature whereas Co/Al₂O₃ shows (as does Co/TiO₂) hydrogen consumption up to much higher temperatures. The support also has an influence on the relative intensities of the diffraction peaks corresponding to the two forms of metallic cobalt (Fig. 17). The samples in which the cobalt is reduced only at higher temperatures show an increased proportion of fcc structure compared to hcp cobalt.

In the case of cobalt based Fischer–Tropsch catalysts the support clearly influences both the reducibility of the precursor oxide and the structure of the metallic phase obtained after reduction. Our study shows that these effects are interrelated, that is, the temperature of reduction primarily determines the fraction of different cobalt structures in the active catalyst. Thus, although it is not yet clear how

the various oxide supports influence the temperature of reduction, the parameters controlling the activity of the final catalyst, should probably be considered in the light of an oxide–support rather than a metal–support interaction. Catalytic result shows that different ratio of fcc and hcp cobalt phases result in the different activities in the CO conversion. Further works are required to decide whether the difference can be attributed to intrinsic activities of the two phases, or to the presence of the defects induced by the presence of the stacking faults in the cobalt particles as suggested by Srinivisan et al. [125].

6.2. Bimetallic systems

Now, we would like to report a preliminary EXAFS and AWAXS study we have performed on the bimetallic Pt–Co/NaY system [126]. The catalysts were prepared by ion exchange. The NaY zeolite support was first stirred with doubly deionised water. Platinum (10 wt.%) was introduced first as [Pt(NH₃)₄](NO₃)₂. After filtering, the Pt/NaY was further exchanged with (1.6 wt.%) Co²⁺ (Co(NO₃)₂). The catalyst was then dried at room temperature, platinum and cobalt contents being determined by X-ray fluorescence [127]. Regarding the EXAFS result, the simulation procedure shows that 4.4 light atoms surround the Pt atoms at a distance of 2.01 Å, which means that the Pt environment is basically unchanged during the impregnation procedure. After the reduction step, the first coordination sphere is made up of 6.5 Pt atoms at 2.72 Å ($\Delta\sigma_{\text{Pt-Pt}} = 0.02 \text{ \AA}$). Thus, the average dia-

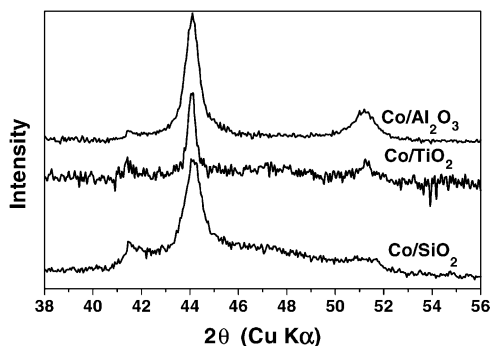


Fig. 17. XRD patterns for the catalytic systems Co/SiO₂ and Co/Al₂O₃ reduced at 873 K and differential intensity for the catalytic systems Co/TiO₂.

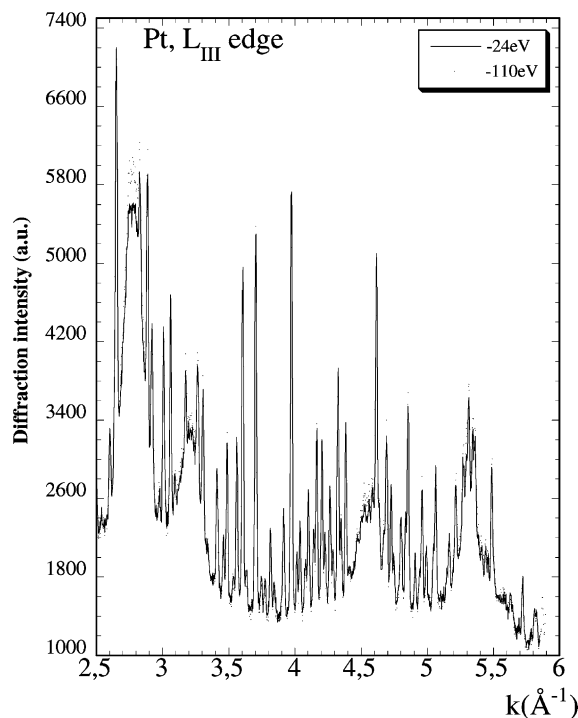


Fig. 18. The diffraction contribution coming from platinum clusters is clearly visible in the raw data after reduction.

meter of the metallic particle seems to be around 15 Å.

After reduction, the diffraction contribution coming from platinum clusters is clearly visible in the raw data (Fig. 18). This experimental fact indicates that classical XRD can be sufficient to obtain structural information on the metallic part of the catalyst. We have seen previously in the case of Co-based catalyst, i.e. for the catalyst having a low metal loading and a well crystallised support it is definitely not the case.

The difference between the two spectra shows an almost featureless residue outside the expected platinum diffraction peaks. This difference has been fitted using Pseudo-Voigt functions for the four main peaks. Using the Scherrer formula (constant equal to 0.94), we obtained an average cluster size of 35 Å with a dispersion between the different peaks (38, 27, 38, 35 Å, respectively, from the 111, 200, 220, 311 peaks). This result (Fig. 19) is compared with the calculated diffraction pattern of a 2057 atoms cluster (cubooctahedra [128] 36 Å diameter).

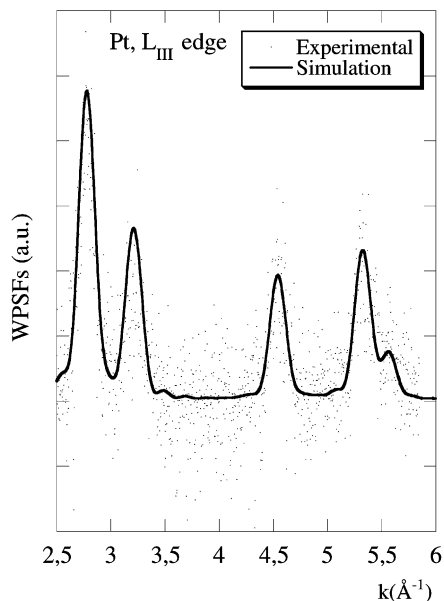


Fig. 19. The experimental result is compared with the calculated diffraction pattern of a 2057 atoms cluster (36 Å diameter).

Based on the EXAFS and diffraction results, two hypotheses can be formulated assuming a significant particle size distribution inside the material. The first assumption is related to the low signal to noise ratio for the difference diffraction spectra. This means that only the contribution of the larger clusters is taken into account. For the absorption spectroscopy, an average over the whole size distribution is obtained, giving rise to a size of 15 Å. Also, we have to underline that the reduced sample was probably reoxidised during the ex situ diffraction experiment. In this process, small particles can be more affected than larger ones, a tendency, which can also explain the difference between EXAFS and diffraction results.

Regarding bimetallic systems the Pt–Mo bimetallic clusters supported on Y zeolite was investigated by Samant et al. [129,130]. This catalytic system shows higher catalytic activity for hydrogenolysis of *n*-butane [131] and CO + H₂ reaction [132] than monometallic clusters of platinum or molybdenum. Such results have been explained by a dual site mechanism by Mo atoms as sites for dissociation of hydrocarbons or CO while Pt atoms are sites for dissociation of dihydrogen and hydrogenation of carbon or the hydrocarbon

fragments. Finally, indirect structural evidence of the presence of bimetallic particles has been given [133]. This structural hypothesis motivated the study by XAS and AWAXS.

In the first paper [129], a reaction cell dedicated to anomalous diffraction experiment is described. The maximum temperature attained in this cell was 573 K while gas could be flowed through the sample. Note also that the sample could be cooled to liquid nitrogen temperature by flowing liquid nitrogen through the sample holder. Regarding the anomalous technique, the dispersion corrections to the atomic scattering factors are evaluated. As we have seen previously, the success of the experiments depends on accurate determination of the atomic factors and thus special attention has to be paid to the different factors $f_0(q)$, $f'(E)$ and $f''(E)$.

In the second paper [130], details have been given on the catalyst preparation as well as on the complete set of experimental EXAFS and AWAXS data. The Pt–Mo/Y zeolite samples were prepared by supporting platinum cluster first on Y zeolite according to the method of Dalla Betta and Boudart [134]. Regarding the Pt/Y zeolite monometallic catalyst, the EXAFS–AWAXS study confirms earlier results that the diameter of Pt clusters is about 10 Å, the metallic entities being located inside the supercages of Y zeolite. The addition of molybdenum does not affect these structural parameters. More precisely, molybdenum atoms are deposited epitaxially on the Pt clusters. The bimetallic clusters show a fcc structure with a nearest neighbour distance of 2.77 Å.

Similar study was performed on bimetallic Pt–Re catalysts by Liang and coworkers [135,136]. As underlined previously the EXAFS spectroscopy cannot give structural evidence regarding the existence or not of bimetallic clusters when the two metals are close in the periodic table (due to the similarity of the backscattering phase and amplitude). In this particular case, only the anomalous scattering can give structural evidence on the presence of bimetallic clusters.

Using the chemical selectivity as in XAS, the data were collected for each metals. Diffraction patterns were collected using X-ray energies 10 and 100 eV below the absorption maxima (white lines) at the L_{III} edges of Pt (11564 eV) and of Re (10535 eV). As usual, the incident intensity I_0 was monitored with

a scintillation detector and the scattered intensity I was measured with an intrinsic Ge detector. The samples which contain equal percentages by weight of Pt and Re were prepared by a co-impregnation procedure [137]. Regarding the acquisition procedure, note that the samples were reduced in flowing H_2 at 475 °C for 2 h, after which they were purged with a stream of helium and cooled to room temperature. They were then passivated by gradual admission of air or oxygen to the helium.

Through a careful analysis of the experimental data, the authors find that the small bimetallic clusters have cores made of platinum atoms with a fcc arrangement on which the rhenium atoms grows epitaxially also in the fcc form. According to surface energy considerations rhenium atoms should be the core of the bimetallic cluster (the heat of sublimation is 135 kcal/mol for platinum and 189 kcal/mol for rhenium). The proposed cluster with a platinum core could be ascribed to the kinetics of the reduction of platinum versus rhenium on the SiO_2 support. Pt probably reduces before rhenium in the original formation of the Pt–Re bimetallic entities. This hypothesis based on the kinetics of reduction has been confirmed by in situ real time studies [138].

6.3. Supported sulfide system

Hydrotreating catalysts for efficient upgrading of crude oil fractions are made of a mixed-sulphide phase supported on oxidic carriers [139–141]. MoS_2 promoted with Ni or Co is an important hydrodesulfurisation (HDS) catalyst used to remove sulfur from petroleum feedstock. Due to the structural characteristics, the usual characterisation techniques, such as transmission electron microscopy, energy-dispersive X-ray emission (EDX), X-ray photoelectron spectroscopy (XPS) and CO chemisorption analysis once again help to confine the problem to the structure of the sulfides particles.

For classical XRD Liang and coworkers [142,143] have established a procedure to interpret the diffraction pattern of poorly crystalline MoS_2 . This method is based on the computation of the XRD pattern through the Debye equation of different structural models based on the hexagonal and the rhombohedral forms of MoS_2 by varying either the size of the crystallites (the number of sandwiched layers, the

number of atoms inside a layer for example) or by introducing different kinds of structural defects. This approach allows identification of the significant features of the diffraction pattern. Finally, an interesting link is established between these calculations and line broadening analysis for the determination of the average crystallite size.

More recently, Tonnerre [81] have performed an EXAFS–AWAXS study of these compounds. Here, the catalyst was an unsupported MoS_2 promoted with Ni and the complete set of data shows clearly that Ni atoms are located on the edge of the MoS_2 layers. Unfortunately, despite a very careful analysis procedure, the weak value of the signal/noise ratio is not sufficient to obtain more information about the location of the nickel atoms.

6.4. Metal oxide materials

Metal oxides metallic and more precisely hydrotalcite-like compounds (HTLcs) have an important industrial application as catalysts precursors and are used in a wide range of reactions, such as basic catalysis, reforming, hydrogenation, oxidation and Ziegler–Nata (for a review see [144]). HTLcs are frequently formed during the synthesis of mixed oxide catalysts via co-precipitation. The structure of HTLcs was first elucidated by Allman and Lohse [145] for the $\text{CO}_3\text{–Mg–Fe}$ system and by Brown and Gastuche for the $\text{CO}_3\text{–Mg–Al}$ system [146].

The catalytic system which has been selected is the $\text{CO}_3\text{–Mg–Ga}$ system, the diffraction contrast between the two cations allowing a more significant study

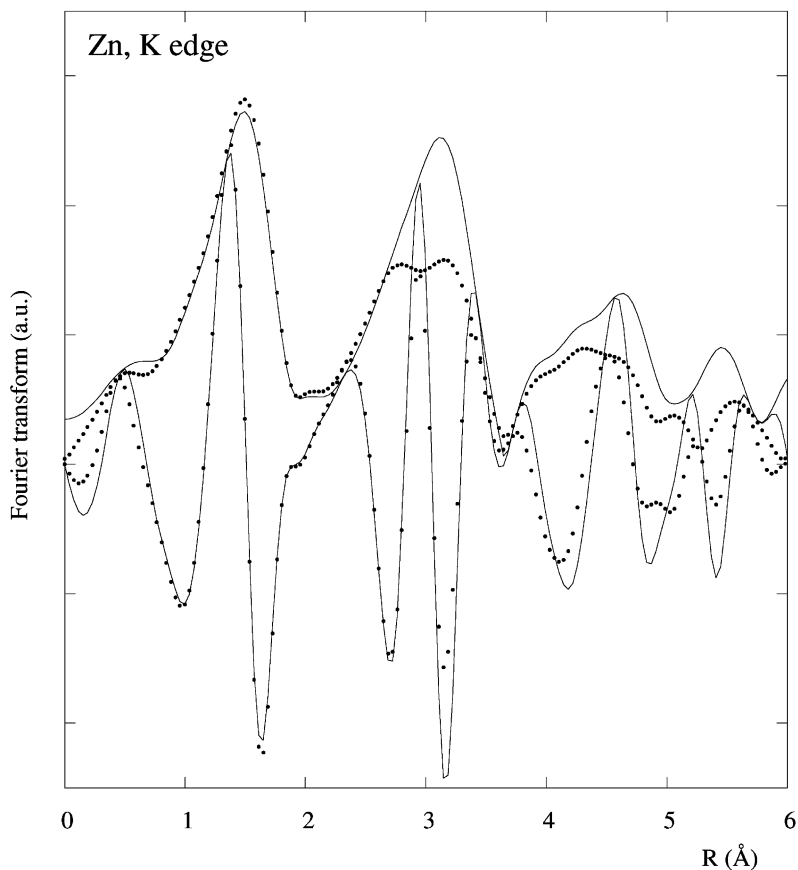


Fig. 20. The Fourier transform of the EXAFS modulations (experimental and calculated spectra) taken at room temperature.

Table 2

Best fit results of the EXAFS oscillations for the spinel ZnAl_2O_4 model compound and the catalyst $\text{ZnAl}_2\text{O}_4/\text{Al}_2\text{O}_3$

Paths	ZnAl_2O_4			$\text{ZnAl}_2\text{O}_4/\text{Al}_2\text{O}_3$				
	N	d (Å)		σ^2 (Å ²)	N	d (Å)		σ^2 (Å ²)
		XRD	EXAFS			XRD	EXAFS	
Zn–O–Zn	4	1.956	1.947 ± 0.005	0.0036 ± 0.0008	4.0 ± 0.5	1.954 ± 0.003	0.004 ± 0.002	
Zn–Al–Zn	12	3.352	3.35 ± 0.01	0.005 ± 0.001	10.9 ± 0.9	3.355 ± 0.004	0.005 ± 0.002	
Zn–O–Zn	12	3.394	3.40 ± 0.02	0.011 ± 0.001	10.9 ± 0.9	3.41 ± 0.02	0.011 ± 0.002	
Zn–Zn–Zn	4	3.501	3.50 ± 0.01	0.009 ± 0.001	0.9 ± 1	3.50 ± 0.01	0.009 ± 0.002	
Zn–Al–O–Zn	24	3.609	3.62 ± 0.02	0.003 ± 0.002	23 ± 3	3.63 ± 0.01	0.003 ± 0.002	
Zn–O–Zn	12	4.272	4.27 ± 0.03	0.002 ± 0.002	6.6 ± 3	4.26 ± 0.02	0.002 ± 0.002	
Zn–Al–O–Zn	24	4.375	4.36 ± 0.03	0.003 ± 0.002	14.3 ± 3	4.34 ± 0.03	0.003 ± 0.002	

versus the system $\text{CO}_3\text{--Mg--Al}$. The preparation procedure which has been reported elsewhere [147] is based on a co-precipitation method at constant pH (pH = 8 for Ni–Al and pH = 9 for Mg–Al and Ga–Al).

First, the crystal chemistry of hydrotalcite-like compounds was investigated by classical diffraction [148]. Then, anomalous diffraction methods as well as XAS [149–151] have been used in order to get a better understanding of their thermal decomposition as well as their chemical properties. At this point, it is important to underline that in this study in situ anomalous diffraction was performed using a cell (A. Paar XRK) which enables in situ high temperature measurements under controlled atmosphere. This apparatus is mechanically very stable, does not introduce temperature dependent aberrations and the sample temperature is within ± 5 K from the set point. Two diffraction patterns were collected on the sample $\text{Mg}/\text{Ga} = 2.0$ at energies 10 and 200 eV below the Ga K absorption edge, fixed at the inflection point measured on the sample itself. The q range explored was $0.54\text{--}9.34 \text{ \AA}^{-1}$. Care was taken to measure air scattering and silicon standard was used to calibrate the wavelength. In fact, the largest uncertainty concerned the f' values set to -3.5 and $9.5e$ far and close to the edge. These values were calculated by the FPRIME program [152].

In this study, the topology of the brucite-type layer as well as the layer stacking arrangement and the intralayer bonding have been determined for the Mg–Al, Mg–Ga and Ni–Al systems. Special attention was paid in the structure determination to the stack-

ing faults which result from of the intergrowth of the rhombohedral and hexagonal polytypes. To attain this goal, the powder XRD pattern has been simulated with the DIFFAX program, which enables modelling of extended planar faults with a statistical recursive approach [153]. Basically, the lack of ordering for systems with highly different cation radii is ascribed

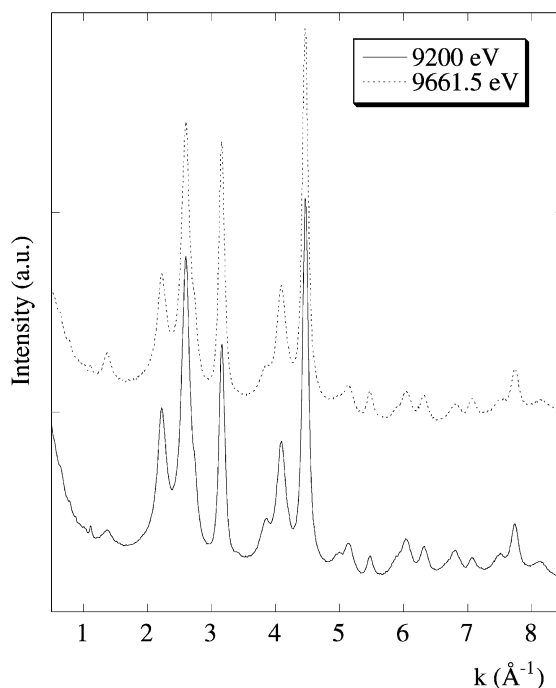


Fig. 21. Diffraction diagram for the catalyst $\text{ZnAl}_2\text{O}_4/\text{Al}_2\text{O}_3$ collected at 9200 eV (line) and 9661.5 eV (dashes).

to the layer compression exhibited by these compounds, which prevent the layer distortion. Note that the stacking arrangement is random for the solids investigated, except for the Mg–Al system which shows a preference for the rhombohedral polytype.

Another example is linked to the decomposition of nitrogen oxides, which are unwanted pollutants in the atmosphere. This reaction has been widely studied and in this context, the copper-exchanged zeolite ZSM-5 is considered as a reference material to reach this goal [154,155]. There are many published studies of catalysts, among which we can distinguish different groups such as metallic particles supported on light oxides (alumina or zeolite) or supported metal oxides.

The material selected for this study [156,157] is a supported catalytic system $\text{ZnAl}_2\text{O}_4/\gamma\text{-Al}_2\text{O}_3$ (atomic composition: 2.3% of Zn, 38.1% of Al and 59.6% of O) provided by Rhodia. Its BET total surface area,

determined with nitrogen adsorption at 77 K, is $131 \text{ m}^2/\text{g}$. The Fourier transform of the EXAFS modulations (experimental and calculated spectra) taken at room temperature are shown in Fig. 20. The result of the fit is summarised in Table 2. The original sample presents an average zinc–oxygen coordination number of 4.0 in line with a tetrahedral coordination. The different coordination numbers as well as the interatomic distances associated with the second shell confirm the fact that the distribution of zinc atoms is spinel-like and indicate a significant loss of Zn^{2+} cations inside the network [158,159].

Regarding anomalous diffraction, Fig. 21 shows the diffraction patterns at each of the two energies we considered here, namely, 9200 and 9661.5 eV. In Fig. 22, the difference in scattered intensities of the catalyst has been compared with the differential intensity of the model compound ZnAl_2O_4 . It is seen that the distribution of zinc atoms in the catalyst is spinel like

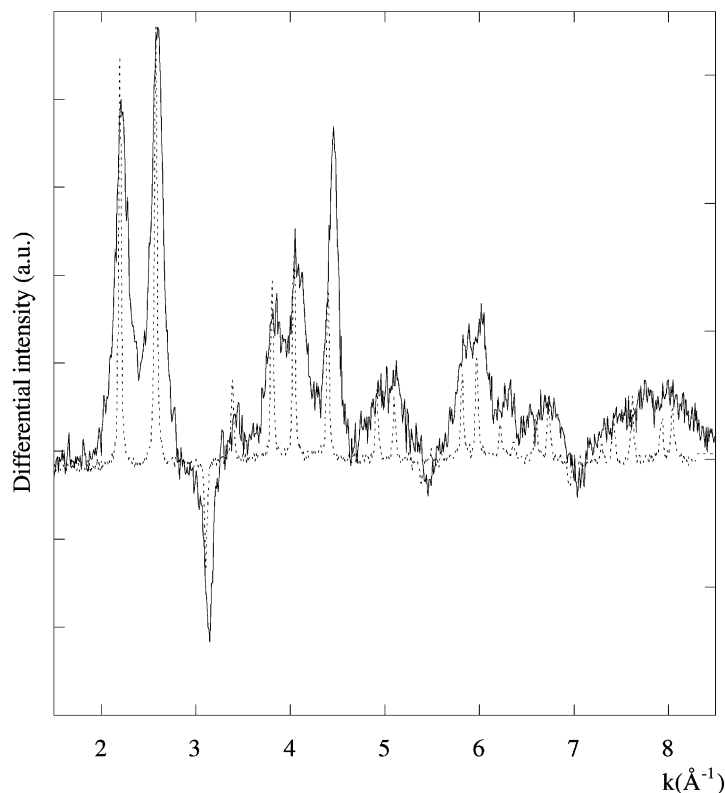


Fig. 22. The difference in scattered intensities of the catalyst has been compared with the differential intensity of the model compound ZnAl_2O_4 .

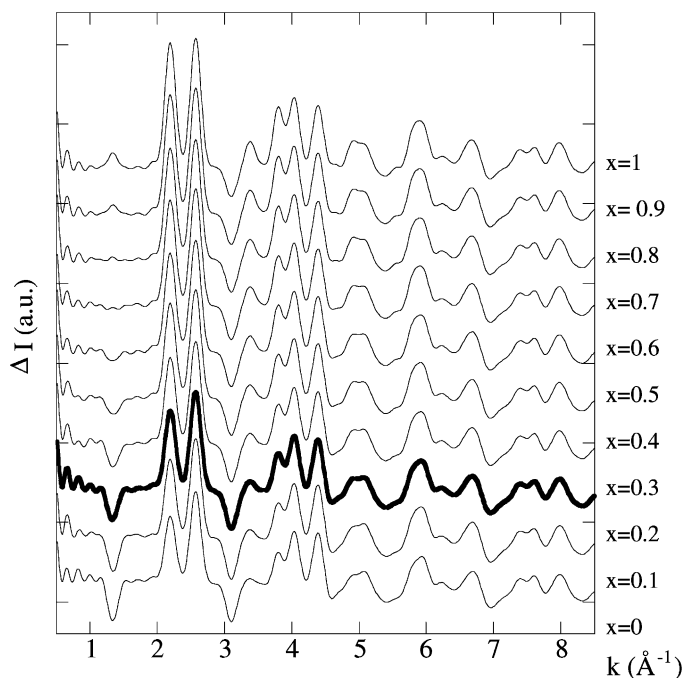


Fig. 23. The second set of numerical simulations based on a Al/Zn substitution starting from the $(\text{Zn}_{1-x}\text{Al}_x)_{\text{Td}}(\text{Al}_2\text{O}_h)\text{O}_4$ composition with $x = 0\text{--}0.9$ were performed.

with a significant contraction of the cell (the peaks are shifted to higher values of k).

Electron microscopy observations form the starting point of the discussion by indicating that the distribution of the zinc atoms in the solid catalyst is inhomogeneous [159]. This qualitative experimental fact is confirmed by the quantitative determination of the local order around zinc atoms given by anomalous scattering experiments and XAS investigations. The local structure around zinc atoms can be considered to be similar to that existing for a ZnAl_2O_4 spinel.

Numerical simulations were performed in order to estimate the coherence length associated with such ZnAl_2O_4 entities and it seems that this parameter is around 40 Å. Nevertheless, some structures, such as the (1 1 1) feature as well as the intensity ratio between the (2 2 0) and the (3 1 1) features are not properly taken into account. Thus, a second set of numerical simulations based on a Al/Zn substitution starting from the $(\text{Zn}_{1-x}\text{Al}_x)_{\text{Td}}(\text{Al}_2\text{O}_h)\text{O}_4$ composition with $x = 0$ to 0.9 were performed. These calculations lead to the differential intensities plotted on Fig. 23. The

experimental results can be accurately reproduced for $x = 0.2$, especially the features at (1 1 1), (2 2 0) and (3 1 1).

7. Conclusion

Through these different examples taken in the literature, we have showed that AWAXS can be considered now as a powerful tool in heterogeneous catalysts characterisation. This technique has allowed the microstructure of catalysts in the active state to be characterised and gives an insight into the parameters controlling the activity of the metallic phase.

From an experimental point of view, in terms of nature of chemical gases which can be passed through the sample as well as temperature or pressure, it is clear that many chemical processes can be mimicked.

Thus, structural and electronic studies are just starting and it is clear that the success will be complete when these synchrotron radiation related techniques

will be used as it is now beginning to be, as a standard tool of scientists as well as engineers.

Acknowledgements

The authors are indebted to Prof. D. Sayers from North Carolina State University (Raleigh, United States), Dr. D. Spanjaard from the Laboratoire de Physique des Solides (Paris XI University, France), Dr. M.C. Desjonqueres (from the CEA-Saclay), Dr. G. Tréglia, Dr. C. Mottet from the CRMC2 (Marseille, France), Dr. F. Garin, Dr. G. Maire from the LERCSI (Strasbourg, France), Dr. Rebours, Dr. Revel for the Institut Français du Pétrole, Dr. A. Seigneurin, Dr. Y. Klur, Dr. A. Pourpoint from Rhodia (Aubervilliers, France), Dr. M. Capelle, Dr. F. Maire, Dr. G. Meunier, Dr. R. Noirot, from PSA Peugeot-Citroën (Centre technique de Belchamp, France) for invaluable discussions on the topic of nanometer scale clusters and Dr. E. Elkaim, Dr. B. Bouchet-Fabre, Dr. J.P. Lauriat, Dr. D. Thiaudiere, Dr. M. Gailhanou from LURE for invaluable discussions on the specificity of XRD using synchrotron radiation. Also, the authors are indebted to the Hungarian Science and Research Fund (T-22117) for financial support and the COST D15/0005/99 program and the Chemistry Department of the CNRS for supporting collaborative program with L.U.R.E synchrotron facilities.

References

- [1] J. Friedel (Ed.), *Physics of Metals 1*, Cambridge University Press, Cambridge, 1978.
- [2] C.R. Henry, *Surf. Sci. Rep.* 31 (1998) 231.
- [3] B.C. Gates, L. Guzzi, H. Knözinger (Eds.), *Metal Clusters in Catalysis*, Elsevier, Amsterdam, 1986.
- [4] G.A. Somorjai (Ed.), *Principles of Surface Chemistry and Catalysis*, Wiley, New York, 1994.
- [5] P. Hohenberg, W. Kohn, *Phys. Rev.* 136B (1964) 864.
- [6] W. Kohn, L. Sham, *Phys. Rev.* 140A (1965) 1133.
- [7] F. Cyrot-Lackmann, F. Ducastelle, *Phys. Rev. Lett.* 27 (1971) 429.
- [8] W.A. Hendrickson, J.R. Horton, D.M. Lemaster, *J. EMBO* 9 (1990) 1965.
- [9] M. Guisnet, J. Barbier, J. Barrault, C. Bouchoule, D. Duprez, G. Perot, C. Montassier (Eds.), *Heterogeneous Catalysis and Fine Chemicals III*, Elsevier, Amsterdam, *Stud. Surf. Sci. Catal.* 78 (1993).
- [10] J.A. Moulijn, P.W.N.M. van Leeuwen, R.A. Van Santen (Eds.), *Catalysis: An Integrated Approach to Homogeneous, Heterogeneous and Industrial Catalysis*, Elsevier, Amsterdam, London, New York, Tokyo, 1993.
- [11] J.M. Thomas, W.J. Thomas (Eds.), *Principles and Practice of Heterogeneous Catalysis*, VCH, New York, 1997.
- [12] M. Shelef, *Chem. Rev.* 95 (1995) 209.
- [13] P. Marecot, A. Fakche, L. Pirault, C. Geron, J. Barbier, G. Mabilon, M. Prigent, *Appl. Catal. B* 5 (1994) 43.
- [14] P. Marecot, L. Pirault, J. Barbier, G. Mabilon, M. Prigent, *Appl. Catal. B* 5 (1994) 57.
- [15] L. Pirault, M. Guerin, P. Marecot, J. Barbier, F. Maire, *Appl. Catal. A* 172 (1998) 249.
- [16] C. Micheaud, P. Marecot, M. Guerin, J. Barbier, *Appl. Catal. A* 171 (1998) 229.
- [17] S. Schneider, D. Bazin, G. Meunier, F. Garin, G. Maire, H. Dexpert, *Appl. Catal. A* 189 (1999) 139.
- [18] S. Schneider, D. Bazin, G. Meunier, R. Noirot, M. Capelle, F. Garin, G. Maire, *Catal. Lett.* 71 (2001) 155.
- [19] M.E. Dry, in: J.R. Anderson, M. Boudart (Eds.), *Catalysis Sciences and Technology*, Vol. 1, Springer, Berlin, 1981, p. 159.
- [20] V.M.H. van Wechem, M.M.G. Senden, in: H.E. Curry-Hyde, R.F. Howe (Eds.), *Natural Gas Conversion II*, Elsevier, Amsterdam, *Stud. Surf. Sci. Catal.* 81 (1994) 43.
- [21] B. Eisenberg, R.A. Fiato, C.H. Mauldin, G.R. Say, S.L. Soled, in: A. Parmaliana, D. Sanfilippo, F. Frusteri, A. Vaccari, F. Arena (Eds.), *Natural Gas Conversion V*, Elsevier, Amsterdam, *Stud. Surf. Sci. Catal.* 119 (1998) 943.
- [22] G.C. Bonds, P.B. Wells, *Adv. Catal.* 15 (1963) 91.
- [23] G.C. Bonds (Ed.), *Catalysis by Metals*, Academic Press, London, 1962.
- [24] G.A. Somorjai, J.M. Thomas (Eds.), *Heterogeneous Catalysis and Fine Chemicals*, Topics in Catalysis, Vol. 13, 2000, p. 3.
- [25] B. Imelik, J.C. Vedrine (Eds.), *Catalyst Characterization: Physical Techniques for Solid Materials*, Plenum Press, Paris, 1994.
- [26] G.A. Somorjai, J.M. Thomas (Eds.), *Catalyst Characterization under Reaction Conditions*, Topics in Catalysis, Vol. 8, 1999, p. 1 and 2.
- [27] EXAFS Spectroscopy in Catalysis, *Top. Catal.* 10 (2000) 3, 4.
- [28] N.S. Guyot-Sionnest, F. Villain, D. Bazin, H. Dexpert, F. Le Peltier, J. Lynch, J.P. Bournonville, *Catal. Lett.* 8 (1991) 283.
- [29] N.S. Guyot-Sionnest, F. Villain, D. Bazin, H. Dexpert, F. Le Peltier, J. Lynch, J.P. Bournonville, *Catal. Lett.* 8 (1991) 297.
- [30] L. Guzzi, D. Bazin, *Appl. Catal. A* 188 (1999) 163.
- [31] R. Prins, D.E. Koningsberger, *X-ray Absorption: Principles, Applications, Techniques of EXAFS, SEXAFS and XANES*, Wiley, New York, 1986.
- [32] G. Sankar, J.M. Thomas, *Top. Catal.* 8 (1999) 1.
- [33] Y. Iwasawa (Ed.), *X-ray Absorption Fine Structure for Catalysts and Surfaces*, World Scientific, London, 1996.
- [34] D. Bazin, L. Guzzi, *Res. Dev. Phys. Chem.* 3 (1999) 387.

- [35] D. Bazin, L. Guzzi, *Appl. Catal. A* 213 (2001) 147.
- [36] D. Bazin, L. Guzzi, *Res. Dev. Phys. Chem.* 4 (2000) 259.
- [37] D. Bazin, D.A. Sayers, J.J. Rehr, *J. Phys. Chem. B* 101 (1997) 11040.
- [38] W.C. Röntgen, *Nature* 53 (1896) 274.
- [39] A.G. Michette, C.J. Buckley (Eds.), *X-ray Science and Technology*, Insitute of Physics, Bristol, 1993.
- [40] A. Guinier, *Théorie et Technique de la Radiocristallographie*, Dunod, Paris, 1964.
- [41] R.W. James, *The Optical Principles of the Diffraction of X-rays*, Bell, London, 1948.
- [42] B.E. Warren, *X-ray diffraction*, Dover, New York, 1990.
- [43] B. Imelik, G.A. Martin, A.J. Renouprez, *Catalyse par les métaux*, CNRS, Paris, 1984.
- [44] J.F. Lepage, *Applied Heterogeneous Catalysis, Design, Manufacture, Use of Solid Catalyst*, Technip, Paris, 1987.
- [45] A.J. Renouprez, H. Jobic, *Catalysis by Metals*, Physique-Springer, Paris, 1997.
- [46] P. Gallezot, *X-ray Techniques in Catalysis*, in: J.R. Anderson, M. Boudart (Eds.), *Catalysis, Science and Technology*, Springer, Berlin, 1984.
- [47] G. Bergeret, *X-ray Powder Diffraction*, in: G. Ertl, H. Knözinger, J. Weitkamp (Eds.), *Handbook of Heterogeneous Catalysis*, VCH, Weinheim, 1997.
- [48] G. Bergeret, in: A.J. Renouprez, H. Jobic (Eds.), *Catalysis by Metals*, Physique-Springer, Paris, 1996.
- [49] Powder diffraction file (PDF), International centre for diffraction data, 12 campus Blvd, Newton square, PA 19073-3273, USA, <http://www.idd.com>.
- [50] C. Hardacre, T. Rayment, R.M. Lambert, *J. Catal.* 158 (1996) 102.
- [51] M.F. Ciruolo, J.C. Hanson, P. Norby, C.P. Grey, *J. Phys. Chem. B* 105 (2001) 2604.
- [52] G. Sankar, P.A. Wright, S. Natarajan, J.M. Thomas, G.N. Greaves, A.J. Dent, B.R. Dobson, C.A. Ramsdale, R.H. Jones, *J. Phys. Chem.* 97 (1993) 9550.
- [53] G. Sankar, J.M. Thomas, C.R.A. Catlow, *Top. Catal.* 10 (2000) 255.
- [54] A.M. Molenbroek, J.K. Norskov, B.S. Clausen, *J. Phys. Chem. B* 105 (2001) 5450.
- [55] B.S. Clausen, H. Topsoe, in: Y. Iwasawa (Ed.), *X-ray Absorption Fine Structure for Catalysts and Surfaces*, World Scientific, Singapore, 1996.
- [56] B.S. Clausen, L. Graek, G. Steffensen, P.L. Hansen, H. Topsoe, *Catal. Lett.* 20 (1999) 23.
- [57] C. Alétru, G.N. Greaves, G. Sankar, *J. Phys. Chem. B* 103 (1999) 4147.
- [58] L.M. Coyler, G.N. Greaves, S.W. Carr, K.K. Fox, *J. Phys. Chem. B* 101 (1997) 10105.
- [59] W. Vogel, H. Knözinger, B.T. Carvill, W.M.H. Sachtler, Z.C. Zhang, *J. Phys. Chem. B* 102 (1998) 1750.
- [60] F.B. Noronha, M. Schmal, R. Fréty, G. Bergeret, B. Moraweck, *J. Catal.* 186 (1999) 20.
- [61] J.F. Faudon, F. Senocq, G. Bergeret, B. Moraweck, G. Clugnet, C. Nicot, A.J. Renouprez, *J. Catal.* 144 (1993) 460.
- [62] A.J. Renouprez, J.F. Trillat, B. Moraweck, J. Massardier, G. Bergeret, *J. Catal.* 179 (1998) 390.
- [63] W. Bras, G.E. Derbyshire, A.J. Ryan, G.R. Mant, A. Felton, R.A. Lewis, C.J. Hall, G.N. Greaves, *NIM A* 326 (1993) 587.
- [64] A. Elhamdaoui, G. Bergeret, J. Massardier, M. Primet, A. Renouprez, *J. Catal.* 148 (1994) 47.
- [65] R.I. Walton, F. Millange, D. O'Hare, A.T. Davies, G. Sankar, C.R.A. Catlow, *J. Phys. Chem. B* 105 (2001) 83.
- [66] D.T. Cromer, J.B. Mann, *Acta Cryst.* A24 (1968) 321.
- [67] F. Hajdu, *Acta Cryst.* A28 (1972) 250.
- [68] C. Tavard, D. Nicolas, M. Rouault, *J. Chem. Phys.* 64 (1967) 540.
- [69] A. Bienenstock, in: Suck, Raoux, Chieux, Riekell (Eds.), "Methods in the Determination of Partial Structure Factors", World Scientific, London, 1993.
- [70] P. Gallezot, M. Avalos-Borja, H. Poppa, K. Heinemann, *Langmuir* 1 (1985) 342.
- [71] G. Bergeret, P. Gallezot, in "Determination de la Structure Atomique des Catalyseurs Solides par Diffraction des Rayons X", Dunod, Paris, 1993.
- [72] V. Gnutzmann, W. Vogel, *J. Phys. Chem.* 94 (1990) 4991.
- [73] N. Hartmann, R. Imbihl, W. Vogel, *Catal. Lett.* 28 (1994) 373.
- [74] W. Vogel, P. Britz, H. Bonnemann, J. Rothe, J. Hormes, *J. Phys. Chem. B* 101 (1997) 11029.
- [75] W. Vogel, B. Rosner, B. Tesche, *J. Phys. Chem.* 97 (1993) 116511.
- [76] M.J. Cooper, *Rep/Prog Phys.* 48 (1985).
- [77] F. Biggs, L.B. Mendelsohn, J.B. Mann, *Atom. Data Nucl. Data Tab.* 16 (1975) 201.
- [78] G. Loupias, J. Chomilier, *Z. Phys. D* 2 (1986) 297.
- [79] G.E. Ice, C.J. Sparks, in: K. Fischer, G. Materlik, C.J. Sparks (Eds.), in: *Proceedings of the International Conference on Anomalous Scattering*, Malente, August 1992.
- [80] D. Raoux, in: Suck, Raoux, Chieux, Riekell (Eds.), "Methods in the Determination of Partial Structure Factors", World Scientific, London, 1993.
- [81] J.M. Tonnerre, Ph.D. thesis, Université Paris VI, Paris, 1992.
- [82] J. De Lima, Ph.D. thesis, Université Paris XI, Paris, 1989.
- [83] D. Udron, Ph.D. thesis, Université Paris VI, Paris, 1990.
- [84] Q. Ma, Ph.D. thesis, Université Paris VI, Paris, 1992.
- [85] N.J. Shevnik, *Philos. Mag.* 35 (1977) 805.
- [86] P.H. Fuoss, P. Eisenberger, W.K. Warburton, A. Bienenstock, *Phys. Rev. Lett.* 46 (1981) 1537.
- [87] S. Ramaseshan, S.C. Abrahams (Eds.), "Anomalous Scattering", Munksgaard, Copenhagen, 1975.
- [88] Suck, Raoux, Chieux, Riekell (Eds.), "Methods in the Determination of Partial Structure Factors", World Scientific, London, 1993.
- [89] Materlik, Sparks, Fischer (Eds.), "Resonant Anomalous X-ray Scattering, Theory and Applications", North Holland, Amsterdam, 1994.
- [90] Y. Waseda, *Novel Application of Anomalous (Resonance) X-ray Scattering for Structural Characterization of Disordered Material*, Series in Physic Science, Springer, Berlin, 1990.
- [91] D.H. Templeton, L.K. Templeton, *Phys. Rev. B* 40 (1989) 6505.

- [92] H. Höln, Z. Phys. 84 (1933) 11.
- [93] H. Höln, Ann. Phys. 18 (1933) 625.
- [94] S. Sasaki, KEK Report 83–82, National Laboratory for High Energy Physics, Japan, 1983.
- [95] D.T. Cromer, D. Liberman, J. Chem. Phys. 53 (1970) 1891.
- [96] D.T. Cromer, D. Liberman, Acta Cryst. A7 (1981) 267.
- [97] M. Marezzio, Acta Cryst. 19 (1965) 284.
- [98] D. Creagh, Phys. Lett. 77A (1980) 129.
- [99] D. Creagh, Phys. Lett. 103A (1984) 52.
- [100] P. Dreier, P. Rabe, W. Malzfeldt, W. Nieman, J. Phys. C17 (1984) 3123.
- [101] B. Lengeler, in: Materlik, Sparks, Fischer (Eds.), "Resonant Anomalous X-ray Scattering, Theory and Applications", North Holland, Amsterdam, 1994.
- [102] D. Bazin, D. Sayers, Jpn. J. Appl. Phys. 32 (2) (1993) 251.
- [103] D. Bazin, D. Sayers, J. Appl. Phys. 32 (2) (1993) 253.
- [104] H. Steiner, P. Giannousis, A. Piusche-Jacques, H.U. Blaser, Top. Catal. 13 (2000) 191.
- [105] S. Brennan, P.L. Cowan, Rev. Sci. Instrum. 63 (1992) 850.
- [106] P. Georgopoulos, J.B. Cohen, J. Catal. 92 (1985) 211.
- [107] K.S. Liang, S.S. Laderman, J.H. Sinfelt, J. Chem. Phys. 86 (1987) 2352.
- [108] V. Favre-Nicolin, S. Bos, J.E. Lorenzo, J.-L. Hodeau, J.-F. Berar, P. Monceau, R. Currat, F. Levy, H. Berger, Phys. Rev. Lett. 87 (2001) 015502.
- [109] C. Bazin, J.M. Dubuisson, A. Labeque, M.P. Level, D. Raoux, M. Sommer, H. Zyngier, J. Chomillier, J. Frouin, Y. Garreau, G. Loupias, J. Tarbes, Rev. Sci. Instr. 60 (1989) 11468.
- [110] G. Nicoli, R. Andouart, C. Barbier, D. Dagneaux, M. Desantis, D. Raoux, in: Proceedings of the Conference on Sociata Italiana Fisica, Vol. 25, 1990, p. 353.
- [111] G. Nicoli, R. Andouart, C. Barbier, D. Dagneaux, M. Desantis, D. Raoux, in: A. Balerna, E. Bernieri, S. Mobilio (Eds.), Proceedings of the International Conference on Progress in X-ray Synchrotron Radiation Research, Rome, 1990, p. 351.
- [112] M. Gailhanou, J.M. Dubuisson, M. Ribbens, L. Roussier, D. Bétaille, C. Créoff, M. Lemonnier, J. Denoyer, C. Bouillot, A. Jucha, A. Lena, M. Idir, M. Bessière, D. Thiaudière, L. Hennet, C. Landron, J.P. Coutures, NIM B, in press.
- [113] P. Ratnasamy, A.J. Leonard, Catal. Rev. Sci. Eng. 6 (1972) 293.
- [114] P. Ratnasamy, A.J. Leonard, L. Rodrigue, J. Fripiat, J. Catal. 29 (1973) 374.
- [115] Q. Ma, J.F. Lee, D.E. Sayers, Phys. B 208/209 (1998) 663.
- [116] A.H. Shamkov, E.M. Moroz, A.L. Chuvilin, NIM B 405 (1998) 470.
- [117] R. Serimaa, V. Etelaniemi, T. Laitalainen, A. Bienenstock, S. Vahvaselka, T. Paakari, Inorg. Chem. 36 (1997) 5574.
- [118] J.K. Barton, C. Caravana, S.J. Lippard, J. Am. Chem. Soc. 101 (1979) 1269.
- [119] T. Okada, T. Shimlura, H. Okuno, Inorg. Chim. Acta 178 (1990) 13.
- [120] C.H. Bartholomew, Catal. Lett. 7 (1990) 27.
- [121] S. Bessel, Appl. Catal. 96 (1993) 253.
- [122] E. Iglesia, S.L. Soled, R.A. Fiato, J. Catal. 137 (1992) 212.
- [123] J. Lynch, O. Ducreux, D. Uzio, B. Rebours, in: Proceedings of 219th ACS National Meeting, San Francisco, 26–31 March 2000, ACS Symposium Preprints, Vol. 45, 2000, p. 325.
- [124] O. Ducreux, J. Lynch, B. Rebours, M. Roy, P. Chaumette, Stud. Surf. Sci. Catal. 119 (1998) 125.
- [125] R. Srinivisan, R.J. de Angelis, P.J. Reucroft, A.G. Dhere, J. Bently, J. Catal. 116 (1989) 144.
- [126] D. Bazin, R. Revel, H. Dexpert, E. Elkaim, J.P. Lauriat, F. Garin, F. Maire, L. Guzzi, G. Lu, J. de Phys. IV (France) 8 (1998) Pr5–263.
- [127] G. Lu, T. Hoffer, L. Guzzi, Catal. Lett. 14 (1992) 207.
- [128] A.L. Mackay, Acta Cryst. 15 (1962) 916.
- [129] M.G. Samant, G. Bergeret, G. Meitzner, P. Gallezot, M. Boudart, J. Phys. Chem. 92 (1988) 3542.
- [130] M.G. Samant, G. Bergeret, G. Meitzner, P. Gallezot, M. Boudart, J. Phys. Chem. 86 (1987) 3547.
- [131] T.M. Tri, J. Massardier, P. Gallezot, B. Imelik, J. Catal. 85 (1984) 244.
- [132] F. Borg, P. Gallezot, J. Massardier, V. Perrichon, C1 Mol. Chem. 1 (1986) 3897.
- [133] T.M. Tri, J.P. Candy, P. Gallezot, J. Massardier, M. Primet, J.C. Vedrine, B. Imelik, J. Catal. 79 (1983) 396.
- [134] R.A. Dalla betta, M. Boudart, in: J.W. Hightower, (Ed.), Proceedings of the 5th International Congress on Catalysis, North Holland, Amsterdam, 1972.
- [135] K.S. Liang, G.J. Hughes, J.H. Sinfelt, Phys. B 158 (1989) 135.
- [136] K.S. Liang, F.Z. Chien, G.J. Hughes, G. Meitzner, J.H. Sinfelt, J. Phys. Chem. 95 (1991) 9974.
- [137] G.A. Meitzner, G.H. Via, F.W. Ilytle, J.H. Sinfelt, J. Chem. Phys. 87 (1987) 6354.
- [138] D. Bazin, H. Dexpert, J. Lynch, J.P. Bournonville, J. Synchr. Rad. 6 (1999) 465.
- [139] B.S. Clausen, F.E. Massoth, in: J.R. Anderson, M. Boudart (Eds.), Catalysis, Science and Technology, Vol. 11, Springer, Berlin, 1996.
- [140] H. Topsoe, B.S. Clausen, Catal. Rev. Sci. Eng. 26 (1984) 395.
- [141] N.Y. Topsoe, H. Topsoe, J. Catal. 84 (1983) 386.
- [142] K.S. Liang, R.R. Chianelli, F.Z. Chen, S.C. Moss, J. Non-Cryst. Solids 79 (1986) 251.
- [143] F.Z. Chen, S.C. Moss, K.S. Liang, R.R. Chianelli, J. de Phys. C4 42 (1981) 273.
- [144] F. Cavani, F. Trifiro, A. Vaccari, Catal. Today 11 (1991) 173.
- [145] R. Allman, H. Lohse, Neues Jahrb. Min. Monatsh 161 (1966).
- [146] G. Brown, M.C. Gastuche, Clay Min. 7 (1967) 177.
- [147] O. Clause, M. Gazzano, F. Trifiro, A. Vaccari, L. Zatorski, Appl. Catal. 73 (1991) 217.
- [148] A.C. Larson, R.B. Von dreele, GSAS Generalized Structure Analysis Package, Document LAUR 86–748, Los Alamos National Laboratory, Los Alamos, 1996.
- [149] M. Bellotto, D. Bazin, M. Bessiere, O. Clause, E. Elkaim, J. Lynch, B. Rebours, in: Proceeding de l'EPDIC IV, Chester, UK, 1995.

- [150] M. Bellotto, B. Rebours, O. Clause, J. Lynch, D. Bazin, E. Elkaim, *J. Phys. Chem.* 100 (1996) 8527.
- [151] M. Bellotto, B. Rebours, O. Clause, J. Lynch, D. Bazin, E. Elkaim, *J. Phys. Chem.* 100 (1996) 8535.
- [152] D.L. Cromer, *Acta Cryst.* 18 (1965) 17.
- [153] M.M.J. Treacy, J.M. Newsam, M.W. Deem, *Proc. R. Soc. London* 433 (1991) 499.
- [154] M. Iwamoto, N.J. Mizumo, *Automot. Eng. (Part D), Proc. Inst. Mech. Eng.* 207 (1993) 23.
- [155] W. Held, A. Konig, T. Richter, L. Puppe, *Soc. Automot. Eng.*, Paper 900496, 1990.
- [156] R. Revel, D. Bazin, H. Dexpert, E. Elkaim, A. Seigneurin, M.A. Perrin, *J. Phys. Chem. B* 104 (2000) 9828.
- [157] R. Revel, Ph.D. thesis, University of Paris XI, Paris, 1997.
- [158] D. Bazin, R. Revel, A.M. Flank, *J. Synchr. Rad.* 6 (1999) 717.
- [159] D. Bazin, R. Revel, *J. Synchr. Rad.* 6 (1999) 483.